



This discussion paper is/has been under review for the journal Atmospheric Measurement Techniques (AMT). Please refer to the corresponding final paper in AMT if available.

Trend analysis of the Aerosol Optical Thickness and Ångström Exponent derived from the global AERONET spectral observations

J. Yoon, W. von Hoyningen-Huene, A. A. Kokhanovsky, M. Vountas, and J. P. Burrows

Institute of Environmental Physics, University of Bremen, Bremen, Germany

Received: 19 July 2011 – Accepted: 12 August 2011 – Published: 18 August 2011

Correspondence to: J. Yoon (yoon@iup.physik.uni-bremen.de)

Published by Copernicus Publications on behalf of the European Geosciences Union.

Title Page

Abstract

Introduction

Conclusions

References

Tables

Figures

◀

▶

◀

▶

Back

Close

Full Screen / Esc

Printer-friendly Version

Interactive Discussion



Abstract

Regular aerosol observations based on well-calibrated instruments have led to a better understanding of the aerosol radiative budget on Earth. In recent years, these instruments have played an important role in the determination of the increase of anthropogenic aerosols by means of long-term studies. Only few investigations regarding long-term trends of aerosol optical characteristics (e.g. Aerosol Optical Thickness (AOT) and Ångström Exponent ($\text{\AA}E$)) have been derived from ground-based observations. This paper aims to derive and discuss linear trends of AOT (440, 675, 870, and 1020 nm) and $\text{\AA}E$ (440–870 nm) using AErosol RObotic NETwork (AERONET) spectral observations. Additionally, temporal trends of Coarse- and Fine-mode dominant AOTs (CAOT and FAOT) have been estimated by applying an aerosol classification based on accurate $\text{\AA}E$ and Ångström Exponent Difference ($\text{\AA}ED$). In order to take into account the fact that cloud disturbance is having a significant influence on the trend analysis of aerosols, we introduce a weighted least squares regression depending on two weights: (1) monthly standard deviation and (2) Number of Observations (NO) per month.

Temporal increase of FAOTs prevails over regions dominated by emerging economy or slash-burn agriculture in East Asia and South Africa. On the other hand, insignificant or negative trends for FAOTs are detected over Western Europe and North America. Over desert regions, both increase and decrease of CAOTs are observed depending on meteorological conditions.

1 Introduction

Aerosols directly influence air quality and solar light extinction as well as indirectly influence the cloud microphysics and cloud radiative forcing (Ackerman et al., 2000; Haywood and Boucher, 2000; Penner et al., 2001; Ramanathan et al., 2001; Léon et al., 2001; Ortore and Francione, 2008). Considerable increase of anthropogenic aerosol is complicating the situation, which leads to the fact that the impact of aerosols

AMTD

4, 5325–5388, 2011

Trend analysis of the Aerosol Optical Thickness

J. Yoon et al.

Title Page

Abstract

Introduction

Conclusions

References

Tables

Figures

◀

▶

◀

▶

Back

Close

Full Screen / Esc

Printer-friendly Version

Interactive Discussion



on climate change still remains at “med-low” or “low” level of scientific understanding (IPCC, 2007).

Recently, several studies (Li et al., 2009; Yu et al., 2009; Zhang et al., 2010; Street et al., 2009; Karnieli et al., 2009; Mishchenko et al., 2007; Mishchenko and Geogdzhayev, 2007; Zhao et al., 2008; Massie et al., 2004) based on well-validated aerosol retrieval algorithms (Remer et al., 2005; Kaufman et al., 1997; Higurashi and Nakajima, 1999; Mishchenko et al., 1999a; Jeong et al., 2005; Higurashi et al., 2000; Stowe et al., 1999; Heidinger et al., 2004; Torres et al., 2002; DiGirolamo and Wilson, 2003; Martonchik et al., 2004; Diner et al., 2006; Martins et al., 2002; von Hoyningen-Huene et al., 2011) using both well-calibrated observations (e.g., Sea-viewing Wide Field-of-view Sensor (SeaWiFS), MEdium Resolution Imaging Spectrometer (MERIS), Multi-angle Imaging SpectroRadiometer (MISR), and Moderate Resolution Imaging Spectroradiometer (MODIS)) and long-term records from space instruments (e.g., Advanced Very High Resolution Radiometer (AVHRR), Total Ozone Mapping Spectrometer (TOMS), and Along Track Scanning Radiometer (ATSR)) have contributed significantly to the understanding of global aerosol trends. Related to these trends, a hypothesis of global brightening or dimming has been discussed as well (Wild et al., 2005, 2007; Ohmura, 2006; Stanhill, 2007; Norris and Wild, 2007). However, aerosol retrievals based on satellite observations often have serious uncertainties caused by instrument calibration and assumptions within the algorithms (Li et al., 2009; Higurashi and Nakajima, 1999; Ignatov and Stowe, 2002). It was found that improvements of the retrieval algorithms need to be accompanied by the reduction of uncertainties due to unscreened clouds, a priori aerosol characteristics (e.g. Single Scattering Albedo (SSA) and phase function), and minimization of the error due to separation techniques to discriminate spectral surface signals (Mishchenko et al., 1999a; Ignatov and Nalli, 2002; Jeong et al., 2005; Myhre et al., 2004; Jeong and Li, 2005; Kahn et al., 2005, 2007; Chen et al., 2008; Kalashnikova and Kahn, 2006; Li et al., 2009; Yu et al., 2009; Zhou et al., 2005; Husar et al., 1997; Haywood et al., 2001; Kokhanovsky and de Leeuw, 2009; von Hoyningen-Huene et al., 2011). For polar-orbiting satellite observations, it is difficult to

Trend analysis of the Aerosol Optical Thickness

J. Yoon et al.

[Title Page](#)

[Abstract](#)

[Introduction](#)

[Conclusions](#)

[References](#)

[Tables](#)

[Figures](#)

◀

▶

◀

▶

[Back](#)

[Close](#)

[Full Screen / Esc](#)

[Printer-friendly Version](#)

[Interactive Discussion](#)



Trend analysis of the Aerosol Optical Thickness

J. Yoon et al.

Title Page

Abstract

Introduction

Conclusions

References

Tables

Figures

◀

▶

◀

▶

Back

Close

Full Screen / Esc

Printer-friendly Version

Interactive Discussion



avoid the bias in aerosol sampling caused by frequent cloud disturbance (Remer et al., 1997; Dubovik et al., 2001; Jeong and Li, 2005; Jeong et al., 2005; Yoon et al., 2011) and coarse temporal resolution of the observation. Therefore, it is also necessary to investigate aerosol trends based on ground-based observations.

The AErosol RObotic NETwork (AERONET) program (<http://aeronet.gsfc.nasa.gov/>) aims to provide a global distribution of aerosol optical properties and to validate satellite retrievals. Despite aerosols below clouds being underrepresented in the AERONET observation database as well (Remer et al., 1997; Dubovik et al., 2001), this network of ground observations provides suitable data for trend analysis of Aerosol Optical Thickness (AOT) based on continuous long-term observations with high temporal resolution as well as good retrieval accuracy (Holben et al., 1998, 2001; Eck et al., 1999; Smirnov et al., 2000). Recently, Karnieli et al. (2009) and de Meij et al. (2010) have discussed AOT trends using long-term AERONET data and have compared them with satellite observations (e.g., Multi-angle Imaging SpectroRadiometer (MISR) and Moderate Resolution Imaging Spectroradiometer (MODIS)) and model simulations (e.g., Co-operative Programme for Monitoring and Evaluation of the Long-range Transmission of Air Pollutants (EMEP), the Region Emission Inventory (REAS) and the Intergovernmental Panel on Climate Change (IPCC, RCP 3PD)). However, they have published no further information about the uncertainty of cloud disturbances and the influences of aerosol classification in the AOT trend analysis.

Cloud disturbances introduce serious uncertainties to trend analysis by decreasing the Number of Aerosol Observations (NO) per temporal interval during persistent cloudiness, thus leading to problems with the statistical representativeness (Yoon, et al., 2011). Therefore, this paper introduces weighted trends using monthly standard deviation and NO to reduce cloud uncertainties in the trend analysis.

Additionally, without applying a classification of aerosol types, the trend studies are only of limited use in order to understand why the aerosol loading changes in time. To support such studies, spectral AOT observations, i.e., the Ångström Exponent (ÅE) (Ångström, 1929), provide a useful quantity to estimate the mean size of particles.

Trend analysis of the Aerosol Optical Thickness

J. Yoon et al.

In general, submicron or supermicron aerosols have higher or lower ÅEs accordingly. However, ÅE is not a perfect indicator to show the exact average size of particles as it also is dependent on aerosol absorption and size distribution. Even though the AERONET inversion process provides useful aerosol optical properties (e.g., volume size distribution and SSA), these could hardly be used to classify aerosols as they are only valid for $AOT(440\text{ nm}) > 0.4$ and solar zenith angle $> 50^\circ$ (Dubovik et al., 2000). Over the last two decades, there have been several studies of ÅE curvature related to the aerosol size distribution (Kaufman, 1993; Eck et al., 1999; O'Neill et al., 2001a, b, 2003, 2005; Schuster et al., 2006; Gobbi et al., 2007). Relationships described in these papers provide a more suitable framework to classify aerosol types using ÅE and Ångström Exponent Difference (ÅED). Therefore, this paper attempts to analyze the temporal trends of Coarse- and Fine-mode dominant AOT (CAOT and FAOT) separately by applying such aerosol classification.

The present study aims to investigate and analyze the long-term trends of AOT, CAOT, FAOT (440, 675, 870, and 1020 nm), and ÅE (440–870 nm) at several AERONET stations. For this purpose, the second section describes in detail the methodology used for the selection of suitable AERONET stations, the weighted least squares regression to consider the cloud uncertainty, and the classification of coarse- and fine-mode dominant aerosols. In the third section, the aerosol trends at the specific AERONET stations are discussed regionally. The conclusions are summarized in the final section.

2 Methodology

For a reliable analysis of the aerosol trends based on the ground observation, new approaches are introduced: (1) the selection criteria for the AERONET stations having sufficient and nearly-complete multi-year data sets, (2) the weighted least squares regression to consider cloud uncertainty, and (3) the classification of coarse- and fine-mode dominant aerosols.

5329



2.1 Selection criteria for suitable AERONET stations

Trend analysis of the Aerosol Optical Thickness

J. Yoon et al.

Title Page

Abstract

Introduction

Conclusions

References

Tables

Figures

◀

▶

◀

▶

Back

Close

Full Screen / Esc

Printer-friendly Version

Interactive Discussion



The AERONET program has provided high quality aerosol products for the past decades over roughly 850 stations globally. However, not all stations distribute a sufficiently large temporal record suitable for a trend analysis. Firstly, we distinguished 5 suitable AERONET stations having a sufficiently large NO record per month. The NO basically depends on the seasonal daytime length, the station's location, the operational instrument status, the cloud disturbance, and the data quality verification process. To get statistically meaningful monthly average values, a large NO is required as the sample average based on a larger sample number is closer to the real average.

10 Therefore, we have defined the minimum NO of 300 per month (10 observations per day) to consider a reliable monthly average value. Another important issue in the trend analysis is the annual completeness of the data set, which needs to consist out of reliable monthly averages. In other words, the absence of continuous monthly averages in the yearly data sets can cause a serious uncertainty in the trend analysis.

15 Basically, we have set up the following set of criteria to choose suitable AERONET stations:

1. The qualified monthly average is calculated with a NO larger than 300 per month (10 observations per day).
2. The sufficiently-complete yearly set consists out of more than seven qualified monthly averages.
- 20 3. A suitable AERONET station needs to have more than five sufficiently-complete years of observation history.

Although a five-years time series may be insufficiently short for a statistically significant trend analysis, it is a first, pragmatic time span to investigate aerosol temporal change from AERONET observations. Figure 1 shows the NO since 1993 for suitable 25 AERONET stations shown in Table 1. Because each station has a different observation

history as well as differently qualified (with respect to the above listed conditions) data sets, it is difficult to perform the investigation of aerosol trends during the same time period. The research periods when the data sets satisfy the selection criteria for each station are indicated by blue fields in Fig. 1. Detailed information about the geolocation and the research periods for the selected AERONET stations are listed in Table 1.

AMTD

4, 5325–5388, 2011

Trend analysis of the Aerosol Optical Thickness

J. Yoon et al.

2.2 Weighted least squares regression

A simple linear model, which is used by minimizing chi-square error statistics, has been adopted in this study. Let Y_t be the monthly AOT averages. The linear trend model is given by the following equation:

$$Y_t = A + BX_t + \epsilon_t, \quad t = 1, \dots, T, \quad (1)$$

where A is a constant term, B is the magnitude of the trend per year ($X_t = t/12$), ϵ_t is the noise, t is the month index, and T is the total number of months. However, as mentioned before, in order to analyze reliable trends, this simple model needs to take into account cloud disturbance.

Each monthly AOT average has been calculated with different NO, which is directly related to the number of cloud occurrence. The trend analysis based on monthly averages during cloudy season may strongly be biased through poor sampling, so that a weighting factor is used to derive the respective trends. Figure 2 depicts the removal ratio of cloud (black line) and quality-unassured (red line) observations of AERONET data. If NO is large enough to ignore the other effects (daytime length, station location, and operational instrument status), then main factors affecting NO could be the cloud disturbance and the data quality verification process. In Fig. 2, the NO of monthly level 2.0 data (n_t) correlate negatively with the cloud removal ratio for most of the stations.

We introduce a weighting factor for the trend analysis.

$$\chi^2(A, B) = \sum_{t=1}^T (wt_t \times (Y_t - A - BX_t))^2 \quad (2)$$

Title Page

Abstract

Introduction

Conclusions

References

Tables

Figures

◀

▶

◀

▶

Back

Close

Full Screen / Esc

Printer-friendly Version

Interactive Discussion



Title Page	
Abstract	Introduction
Conclusions	References
Tables	Figures
◀	▶
◀	▶
Back	Close
Full Screen / Esc	
Printer-friendly Version	
Interactive Discussion	

where, wt_t ($= \sqrt{n_t}/\sigma_t$) is the monthly weighting factor defined as ratio of NO (n_t) and monthly standard deviation (σ_t). Monthly standard deviation is by itself a suitable weight as it statistically shows the representativeness (variability or diversity) of the average. In the following we will estimate the cloud uncertainty through the comparison between the weighted and unweighted trends.

2.3 Classification of coarse- and fine-mode dominant aerosols

In order to quantify the change in anthropogenic (generally, fine-mode dominant) and natural (coarse-mode dominant) aerosols, an aerosol classification needs to be applied as well. The AERONET inversion process (Dubovik and King, 2000; Dubovik et al., 2000, 2001, 2002, 2006; Sinyuk et al., 2007) generates various aerosol characteristics such as volume size distribution and SSA. However, the data are only provided for the following conditions: $AOT(440\text{ nm}) > 0.4$ and solar zenith angle $> 50^\circ$ (Dubovik et al., 2000). Figure 3 shows the normalized frequency of AOT (440 nm) and solar zenith angle at the selected AERONET stations. Generally, the normalized frequency (histogram) distributions of AOT (440 nm) are skewed and have long tails towards larger values of AOT. The percentage of AERONET level 2.0 inversion data to the total observations is indicated as a pie chart on the lower-left hand side in Fig. 3. In most cases, it is difficult to use the AERONET inversion data for aerosol classification because of a low proportion to total observations meeting the conditions mentioned above. Alternatively, we propose a classification of coarse- and fine-mode dominant aerosols using ÅE and ÅED retrievals from AERONET direct sun data. ÅE and ÅED are defined as:

$$\text{ÅE} = -\frac{\ln(\tau_{440\text{ nm}}/\tau_{870\text{ nm}})}{\ln(440\text{ nm}/870\text{ nm})} \quad (3)$$

$$\text{ÅED} = -\frac{\ln(\tau_{440\text{ nm}}/\tau_{675\text{ nm}})}{\ln(440\text{ nm}/675\text{ nm})} + \frac{\ln(\tau_{675\text{ nm}}/\tau_{870\text{ nm}})}{\ln(675\text{ nm}/870\text{ nm})} \quad (4)$$

where, τ_λ is AOT at wavelength (λ).

**Trend analysis of the
Aerosol Optical
Thickness**

J. Yoon et al.

[Title Page](#)[Abstract](#)[Introduction](#)[Conclusions](#)[References](#)[Tables](#)[Figures](#)[|◀](#)[▶|](#)[Back](#)[Close](#)[Full Screen / Esc](#)[Printer-friendly Version](#)[Interactive Discussion](#)

Several investigations have been previously devoted to the curvature of the spectral dependence of the optical depth in order to derive more accurate aerosol size information. For example, Kaufman (1993) found that the spectral curvature shows a transition from mixed accumulation and coarse particle modes to a dominant accumulation mode. Eck et al. (1999) investigated the wavelength dependence of the optical depth of biomass burning, urban, and desert dust aerosols. O'Neill et al. (2001a, b, 2003, 2005) and Schuster et al. (2006) presented a detailed analysis and compared simulations and observations in order to investigate the relationship between aerosol size distribution and spectral dependence of the AOT. Gobbi et al. (2007) have set up a useful straight-forward graphical framework applicable to classify aerosol properties (effective radius and fine mode fraction to total AOT) using ÅED as a measure of the curvature. They have applied the graphical framework to AERONET data and were able characterize different aerosol types such as pollution, mineral dust, and biomass burning. However, none of the above mentioned publications involved their methods in trend analyses.

Here, we build up a similar classification as Gobbi et al. (2007). With Fig. 4, using the Mie theory, we tested the relationship between ÅE and ÅED simulated with many bimodal volume size distributions consisting out of mode radii, widths, fine volume fractions, and refractive indices shown Table 2. Negative ÅED shows a high proportion of fine mode aerosol for the same ÅE. In this study, we set up the classification using both ÅE and ÅED to consider aerosol mean size and fine volume fraction together.

In this study, coarse-mode (fine-mode) dominant aerosols are classified by lower (higher) values than ÅE of at least 1.0 (Kaufman, 1993) and a fine volume fraction of 50 %. For positive ÅED values (larger than 0.17), the fine volume fraction of 50 % scatters significantly (Fig. 4). In order to be able to classify even for these values, additional Mie simulations (Mishchenko et al., 1999b, 2002) have been performed based on aerosol characteristics of typical aerosols (urban-industrial and mixed, biomass burning, desert dust, oceanic from Dubovik et al. (2001)) shown in Table 3 and Fig. 5. The red line shown in Fig. 5, especially the upper part relevant for positive ÅED, could be

Trend analysis of the Aerosol Optical Thickness

J. Yoon et al.

Title Page

Abstract

Introduction

Conclusions

References

Tables

Figures

◀

▶

◀

▶

Back

Close

Full Screen / Esc

Printer-friendly Version

Interactive Discussion



(Beijing (C 64 % > F 36 %) and Shirahama (C 44 % < F 56 %)). The classification is not applicable to data observed at Mauna_Loa and Sevilleta because most AOTs (440 nm) over these stations were less than 0.15.

By applying the aerosol classification, it is possible to analyze more reliable trends
5 separately for coarse- and fine-mode dominant aerosols. However, stations dominated by coarse-mode aerosols (such as Banizoumbou, Dakar, Ouagadougou, and Solar_Village) or those with an extremely small aerosol load (such as Mauna_Loa and Sevilleta) are neglected.

3 Trend analysis

10 For this part of study, we have selected fifteen AERONET stations providing datasets meeting the requirements specified in Sect. 2.1. In the following sections, the trends for the stations located in several regions (Western Europe, West Africa, South Africa, Middle East, East Asia, North America, and Free troposphere/Pacific) are discussed. The trends of ÅE (440–870 nm) and AOT (440 nm) at the AERONET stations are shown
15 in Fig. 7. For clarity, the error bar is scaled by a factor 10 of the standard error ($\sigma_t / \sqrt{n_t}$), which is inversely used for the weighted trend analysis. Comparison between unweighted (blue line and text on the left upper part) and weighted trends (red line and text on the right upper part) allows to estimate the uncertainty caused by cloud disturbance in the trend analysis.

20 In this paper, we would like to discuss the aerosol trends mainly on the basis of the weighted trend of AOT (440 nm) and ÅE (440–870 nm). As previously mentioned, we also introduce a classification of coarse- and fine-mode dominant aerosols based on the Mie theory in the trend analysis in Fig. 9. Finally, the weighted trends of ÅE (440–870 nm), AOT, CAOT, and FAOT (440 nm) over all AERONET stations are summarized in Figs. 8 and 10.
25

Title Page	
Abstract	Introduction
Conclusions	References
Tables	Figures
◀	▶
◀	▶
Back	Close
Full Screen / Esc	
Printer-friendly Version	
Interactive Discussion	



Trend analysis of the Aerosol Optical Thickness

J. Yoon et al.

[Title Page](#)

[Abstract](#)

[Introduction](#)

[Conclusions](#)

[References](#)

[Tables](#)

[Figures](#)

◀

▶

◀

▶

[Back](#)

[Close](#)

[Full Screen / Esc](#)

[Printer-friendly Version](#)

[Interactive Discussion](#)



3.1 Western Europe

The averages of ÅE shown in Fig. 7, for Avignon ($\langle \text{ÅE} \rangle = 1.43$) and Ispra ($\langle \text{ÅE} \rangle = 1.51$) over Western Europe, were mainly influenced by urbanization and industrial pollutants, such as ammonium salts of sulphate and nitrate (Robles González et al., 2000; Benkovitz et al., 1996). The seasonal variation of ÅE is small as the major source during the year is industrial pollutant. On the other hand, the AOTs over Western Europe exhibit a significant seasonal variation, which is increasing from spring to summer and decreasing from autumn to winter (Fig. 7). Basically, the AOT depends on the aerosol extinction coefficient (influenced, e.g., by aerosol types, emission intensity, and relative humidity) and boundary layer height. Especially industrial pollutants composed of sulphur are enhanced during summer due to stronger solar radiation (Marmer et al., 2007; Karnieli et al., 2009). Additionally, the absence of removal process (e.g., rain/monsoon) as well as a high boundary layer height causes higher AOTs over Europe in summer (Gerasopoulos et al., 2003; Bergamo et al., 2008; Venzac et al., 2009). The weighted AOT trends over both stations are insignificant or decreasing (+0.98%/year at Avignon and -2.30%/year at Ispra), most likely due to strict environmental regulations for mitigating climate change and improving air quality (Smith et al., 2001; Streets et al., 2006; Zhao et al., 2008). There is little difference between weighted and unweighted trends of ÅE and AOT (Fig. 7). The AOTs at Avignon and Ispra over Western Europe, where most aerosols are classified as fine-mode dominant caused by industrial activity, tend to be negligible or decreasing (+0.24%/year at Avignon and -2.30%/year at Ispra as shown in Fig. 9).

3.2 West Africa

Mineral dust mainly from the Saharan and Sahel regions is the most abundant aerosol type over West Africa influencing Banizoumbou, Dakar, and Ouagadougou stations year-round (Prospero and Lamb, 2003; Washington and Todd, 2005; Moulin and Chiapello, 2004; Reeves et al., 2010). Besides, biomass burning is frequently advected

**Trend analysis of the
Aerosol Optical
Thickness**

J. Yoon et al.

[Title Page](#)[Abstract](#)[Introduction](#)[Conclusions](#)[References](#)[Tables](#)[Figures](#)[|◀](#)[▶|](#)[Back](#)[Close](#)[Full Screen / Esc](#)[Printer-friendly Version](#)[Interactive Discussion](#)

by the West African monsoon in summer from central Africa (Hao and Liu, 1994). Additionally, low AOT might occur as a result of efficient wet removal of aerosol particles due to heavy precipitation (Reeves et al., 2010; Huang et al., 2009). In Fig. 7, series of these phenomena over West Africa represent the seasonal pattern in ÅE and AOT. Insignificant or decreasing trends of dust aerosol due to decreasing dust activity (Evan et al., 2007) are observed over most stations in West Africa (+0.22%/year at Banizoumbou, -1.53%/year at Dakar, and -1.95%/year at Ouagadougou), which is consistent with the results from the Global Aerosol Climatology Project (GACP) data (Mishchenko and Geogdzhayev, 2007; Mishchenko et al., 2007), in situ measurement, AVHRR, and TOMS observations (Chiapello and Moulin, 2002; Chiapello et al., 2005; Zhao et al., 2008). The weighted trends of ÅE and AOT at Dakar and at Ouagadougou are different compared to unweighted trends due to frequent cloud disturbance. CAOT trends over West Africa (+0.29%/year at Banizoumbou, -1.47%/year at Dakar, and -1.86%/year at Ouagadougou in Fig. 9) are generally similar with AOT trends.

3.3 South Africa

ÅE as well as AOT over stations in South Africa (i.e., Mongu and Skukuza) exhibit a strong seasonality due to pronounced wet and dry seasons (see Fig. 7), and the presence of biomass burning aerosol (Tyson, 1986; Swap et al., 1996). Biomass burning leads to a large aerosol load in warm and dry seasons. The cloud uncertainty in the trend analysis is insignificant because the biomass burning generally happens before the beginning of the rain seasons. A noticeable increase of AOT at Mongu (+2.26%/year) is most likely affected by biomass burning (Mishchenko and Geogdzhayev, 2007; Zhao et al., 2008). Accordingly, positive trends of FAOT over South Africa are observed (+1.76%/year at Mongu and +0.75%/year at Skukuza) in Fig. 9.

3.4 Middle East

The stations SEDE_BOKER and Solar_Village are located within the Middle East and provide a long record of measurements because of stable, clear-sky weather conditions (Basart et al., 2009) (see Fig. 2). In this region, aerosol size and composition are dominated by the regional petroleum industry (Zhao et al., 2008; Basart et al., 2009) and mineral dust which is transported from the Anatolian plateau, Sahara, Negev, and Arabian deserts (Andreae et al., 2002; Kubilay et al., 2003; Derimian et al., 2006; Basart et al., 2009; Sabbah et al., 2001, 2006; Smirnov et al., 2002; Tafuro et al., 2006; Sabbah and Hasan, 2008). The latter explains the clear periodical pattern of ÅE and AOT seen in Fig. 7. The AOT over SEDE_BOKER tend to decrease ($-2.16\text{ \%}/\text{year}$) due to a decrease in small particles (Karnieli et al., 2009), while AOT over Solar_Village show a strong increase ($+3.29\text{ \%}/\text{year}$) in the weighted trend probably related to change of atmospheric conditions (e.g., increase of wind speed and relative humidity) (Sabbah and Hasan, 2008). Interestingly, there are severe differences between the unweighted and weighted trends at both stations due to a large standard error caused by high variability of ÅE and AOT. The weighted trend of CAOT of SEDE_BOKER and Solar_Village is -2.30 \% and $+3.39\text{ \%}/\text{year}$ respectively (as seen in Fig. 9).

3.5 East Asia

Many emerging economies are found in East Asia, where, as a consequence, large amounts of anthropogenic aerosols are emitted. Additionally, mineral dust from the deserts in Mongolia and in Western and Northern China (mainly the Taklimakan and Badain Juran deserts) contributes around 70 % of the total dust emissions in mid-latitude regions. Rapid desertification caused by climatic variation and human activities additionally increases the aerosol burden due to mineral dust transport (Zhang et al., 2003). ÅE and AOT at Beijing in Fig. 7 exhibit very clear seasonal cycles, which have been explained by the complex combination of natural and anthropogenic aerosols, stagnant synoptic meteorological patterns, secondary aerosol formation, and

[Title Page](#)[Abstract](#)[Introduction](#)[Conclusions](#)[References](#)[Tables](#)[Figures](#)[|◀](#)[▶|](#)[◀](#)[▶](#)[Back](#)[Close](#)[Full Screen / Esc](#)[Printer-friendly Version](#)[Interactive Discussion](#)

**Trend analysis of the
Aerosol Optical
Thickness**

J. Yoon et al.

[Title Page](#)[Abstract](#)[Introduction](#)[Conclusions](#)[References](#)[Tables](#)[Figures](#)[|◀](#)[▶|](#)[◀](#)[▶|](#)[Back](#)[Close](#)[Full Screen / Esc](#)[Printer-friendly Version](#)[Interactive Discussion](#)

hygroscopic growth (Kotchenruther et al., 1999; Dubovik et al., 2001; Kim et al., 2007). Because of industrialization, urbanization, and desertification over East Asia in the last twenty years, the aerosol loading over Beijing increased rapidly and the magnitude of the weighted trend is +4.59%/year. This trend is consistent with many previous studies (Streets et al., 2000, 2003, 2006; Smith et al., 2001, 2003; Massie et al., 2004; Mishchenko and Geogdzhayev, 2007; Zhao et al., 2008). The weighted trend is larger than the unweighted one (+1.06%/year), as there are smaller weighting factors during summer (in Beijing, frequent cloud disturbance and strong mineral dust events are characteristic during summer time). Shirahama is in the middle of Japan, far from large cities, facing the Pacific Ocean (Mukai et al., 2006). Hence, maritime aerosol is predominant, but there are occurrences of mineral dust and/or industrial aerosol transported by strong westerly winds from China (Sano et al., 2003; Mukai et al., 2005). The seasonal cycles of ÅE and AOT in Fig. 7 are similar to those at Beijing due to similar meteorological conditions and aerosol sources. The upward trend of AOT is small (+0.44%/year), while FAOT increases (+2.07%/year) clearly. Due to comparatively small NO over Shirahama, only slight differences between weighted and unweighted trends of ÅE and AOT are observed all year round (see Fig. 2). The magnitude of the trends is, after classification, small for Shirahama, +1.83%/year for CAOT and +0.28%/year for FAOT. Such increase is also observed for Beijing, but is even more pronounced for weighted trends of CAOT and FAOT with increases of +5.12% and +8.72%/year, respectively.

3.6 North America

The stations GSFC and MD_Science_Center are located on urban and built-up land, while Sevilleta is positioned at shrub land over North America (Liu et al., 2004). Therefore, they basically measure aerosols from different sources. The main aerosol type measured at GSFC and MD_Science_Center is due to urban-industrial pollution, mainly due to vehicles and industries. The seasonal cycles of ÅE and AOT in Fig. 7 demonstrate that the variabilities are strongly dependent on the combination of

[Title Page](#)[Abstract](#)[Introduction](#)[Conclusions](#)[References](#)[Tables](#)[Figures](#)[|◀](#)[▶|](#)[Back](#)[Close](#)[Full Screen / Esc](#)[Printer-friendly Version](#)[Interactive Discussion](#)

natural and anthropogenic aerosols, fuel types, emission characteristic, relative humidity, boundary layer depth, and scavenging by precipitation (Glen et al., 1996; Chen et al., 2001; Dubovik et al., 2001; Andronache, 2004). The negative trends of AOT ($-0.54\text{ \%}/\text{year}$ at GSFC and $-0.88\text{ \%}/\text{year}$ at MD_Science_Center) are consistent with the decrease of industrial emissions in the United States of America (Smith et al., 2001; Streets et al., 2006; Zhao et al., 2008).

Sevilleta station measures a relatively small aerosol loading for the considered time span. The weighted trends are strongly negative ($-1.66\text{ \%}/\text{year}$ for \AA E and $-3.79\text{ \%}/\text{year}$ for AOT), clearly different from the unweighted ones ($+0.43\text{ \%}/\text{year}$ for \AA E and $+3.28\text{ \%}/\text{year}$ for AOT). In most cases of monthly averaged AOT at Sevilleta, the values are lower than 0.15, so that the classification for the trend analysis was not applied to data of this station. The majority of retrieved aerosol type at GSFC and MD_Science_Center is fine-mode, and the weighted trends of FAOT are -0.45 \% and $-0.18\text{ \%}/\text{year}$, respectively (see Fig. 9).

3.7 Mauna Loa

Aerosols measured at Mauna Loa (alt. $\sim 3397\text{ m}$) in the Pacific are representative for free tropospheric aerosols. However, the stations is also under some influence of long-range transport of Asian mineral dust and pollution (Dubovik et al., 2001). The free troposphere is characterized by being almost cloud-free in the subsiding branch of the Hadley cell as well as a pathway for long-distance transport of aerosols (Garstang and Fitzjarrald, 1999; Schmeissner et al., 2011). In most cases, free tropospheric AOT (440 nm) does not exceed values of 0.05 except when affected by volcano eruption or transported mineral dust and pollution. Therefore, it is difficult to analyze size and type, as the error of \AA E is larger than 30 % with AOTs smaller than 0.15 (Gobbi et al., 2007). The main factors affecting the seasonal pattern of AOT are most likely long-range transported aerosols and seasonal meteorological conditions; the AOT trend for this station is positive ($+1.73\text{ \%}/\text{year}$).

**Trend analysis of the
Aerosol Optical
Thickness**

J. Yoon et al.

[Title Page](#)[Abstract](#)[Introduction](#)[Conclusions](#)[References](#)[Tables](#)[Figures](#)[◀](#)[▶](#)[Back](#)[Close](#)[Full Screen / Esc](#)[Printer-friendly Version](#)[Interactive Discussion](#)

- The relative weighted trends of ÅE (440–870 nm), AOT, CAOT, and FAOT (440 nm) in percent for the above described stations are indicated on the global map in Figs. 8 and 10. In general, total aerosol load tends to decrease over Western Europe and North America, while it is increasing over West and South Africa, Middle East, and East Asia.
- 5 The classification of aerosol types explains why the aerosol load changes in time. Consistent with our expectations, fine-mode dominant aerosol loading, primarily created by human activities, is decreasing over those countries having strict environmental regulations, while it is increasing over regions in emerging economies without such strict environmental regulations. Temporal variation of the loading of coarse-mode dominant aerosol depends strongly on meteorological conditions varying with climate change. In particular, those AERONET stations close to the regions where rapid desertification plays a role are characterized by a considerable increase of coarse-mode dominant aerosol. All values (i.e., average, unweighted, and weighted trends of ÅE, AOT, CAOT, and FAOT) are shown in Tables 4 and 5.

15 4 Summary and conclusion

In this study, long-term trends of the Ångström Exponent (ÅE) (440–870 nm), Aerosol Optical Thickness (AOT), Coarse-, and Fine-mode dominant AOTs (CAOT and FAOT) (440, 675, 870, and 1020 nm) observed at several AERONET stations have been analyzed. Firstly, suitable AERONET stations providing sufficiently long-term data series are chosen in order to make a meaningful trend analysis. Unfortunately, the research periods are different for each AERONET station due to the different observation history and condition (see Table 1 and Fig. 1). Weighted trends have been derived utilizing monthly standard deviation and Number of Observations (NO) providing an estimate of trend uncertainty (primarily) due to cloud disturbance. For example, if there was a high variability of aerosol loading for a small NO, then significant difference between unweighted and weighted trends is observed.

In general, cloud-free aerosol trends in this study are consistent with results from other papers (Smith et al., 2001; Streets et al., 2006; Zhao et al., 2008; Evan et al., 2007; Mishchenko and Geogdzhayev, 2007; Mishchenko et al., 2007; Chiapello and Moulin, 2002; Chiapello et al., 2005; Karnieli et al., 2009). The aerosol classification using AE and AED from AERONET spectral observations has been useful to investigate trends of Coarse- and Fine-mode dominant AOTs. The aerosol load is increasing over the stations in/near emerging economies or biomass burning regions and decreasing over the countries under strict environmental regulations. After applying classification, these trends are more apparent. Except Western Europe and North America, most of the considered regions have positive trends of fine-mode dominant aerosol. In particular, the weighted trends of both CAOT and FAOT at Beijing over East Asia show considerable increases. Due to the high density of population in many strongly polluted areas (e.g., 1300 people per 1 km^2 in Beijing) and the correlation between aerosol load and mortality (Foster and Kumar, 2011), there is an urgent need for measures to reduce the aerosol load in large urban agglomerations (aka megacities) worldwide similar to those already introduced in Western Europe and North America.

Acknowledgements. This work was supported in part by the CityZen project (megaCITY – Zoom for the Environment: EU Framework Programme 7 of European Commission), the DFG Project Terra, and the University of Bremen. The authors would like to thank NASA AERONET team for the provision of aerosol optical properties data. We are thankful to M. I. Mishchenko for providing the Mie code used in this study. I especially wish to express my gratitude to J. S. Jang, who encouraged me in the work.

References

- Ackerman, A. S., Toon, O. B., Stevens, D. E., Heymsfield, A. J., Ramanathan, V., and Welton, E. J.: Reduction of tropical cloudiness by soot, *Science*, 288, 1042–1047, 2000.
Andreae, T. W., Andreae, M. O., Ichoku, C., Maenhaut, W., Cafmeyer, J., Karnieli, A., and Orlovsky, L.: Light scattering by dust and anthropogenic aerosol at a remote site in the Negev desert, Israel, *J. Geophys. Res.*, 107(D2), 4008, doi:10.1029/2001JD900252, 2002.

5 4, 5325–5388, 2011

Trend analysis of the Aerosol Optical Thickness

J. Yoon et al.

[Title Page](#)

[Abstract](#)

[Introduction](#)

[Conclusions](#)

[References](#)

[Tables](#)

[Figures](#)

◀

▶

◀

▶

[Back](#)

[Close](#)

[Full Screen / Esc](#)

[Printer-friendly Version](#)

[Interactive Discussion](#)



**Trend analysis of the
Aerosol Optical
Thickness**

J. Yoon et al.

- Andronache, C.: Estimates of sulfate aerosol wet scavenging coefficient for locations in the Eastern United States, *Atmos. Environ.*, 38, 795–804, 2004.
- Ångström, A.: On the atmospheric transmission of sun radiation and on dust in the air, *Geograf. Ann. Deut.*, 11, 156–166, 1929.
- Basart, S., Pérez, C., Cuevas, E., Baldasano, J. M., and Gobbi, G. P.: Aerosol characterization in Northern Africa, Northeastern Atlantic, Mediterranean Basin and Middle East from direct-sun AERONET observations, *Atmos. Chem. Phys.*, 9, 8265–8282, doi:10.5194/acp-9-8265-2009, 2009.
- Benkovitz, C. M., Scholtz, M. T., Pacyna, J., Tarrason, L., Dignon, J., Voldner, E. C., Spiro, P. A., Logan, J. A., and Graedel, T. E.: Global gridded inventories of anthropogenic emissions of sulphur and nitrogen, *J. Geophys. Res.*, 101, 29239–29253, 1996.
- Bergamo, A., Tafuro, A. M., Kinne, S., De Tomasi, F., and Perrone, M. R.: Monthly-averaged anthropogenic aerosol direct radiative forcing over the Mediterranean based on AERONET aerosol properties, *Atmos. Chem. Phys.*, 8, 6995–7014, doi:10.5194/acp-8-6995-2008, 2008.
- Chen, L.-W. A., Doddrige, B. G., Dickerson, R. R., Chow, J. C., Mueller, P. K., Quinn, J., and Butler, W. A.: Seasonal variations in elemental carbon aerosol, carbon monoxide and sulfur dioxide: Implications for sources, *Geophys. Res. Lett.*, 28(9), 1711–1714, 2001.
- Chen, W.-T., Kahn, R., Nelson, D., Yau, K., and Seinfeld, J.: Sensitivity of multi-angle imaging to optical and microphysical properties of biomass burning aerosols, *J. Geophys. Res.*, 113, D10203, doi:10.1029/2007JD009414, 2008.
- Chiapello, J. and Moulin, C.: TOMS and Meteosat satellite records of the variability of Saharan dust transport over the Atlantic during the last two decades (1979–1997), *Geophys. Res. Lett.*, 29(8), 1176, doi:10.1029/2001GL013767, 2002.
- Chiapello, I., Moulin, C., and Prospero, J. M.: Understanding the long-term variability of African dust transport across the Atlantic as recorded in both Barbados surface concentrations and large-scale total ozone mapping spectrometer (TOMS) optical thickness, *J. Geophys. Res.*, 110, D18S10, doi:10.1029/2004JD005132, 2005.
- de Meij, A., Pozzer, A., and Lelieveld, J.: Global and regional trends in aerosol optical depth based on remote sensing products and pollutant emission estimates between 2000 and 2009, *Atmos. Chem. Phys. Discuss.*, 10, 30731–30776, doi:10.5194/acpd-10-30731-2010, 2010.
- Derimian, Y., Karnieli, A., Kaufman, Y. J., Andreae, M. O., Andreae, T. W., Dubovik, O.,

[Title Page](#)[Abstract](#)[Introduction](#)[Conclusions](#)[References](#)[Tables](#)[Figures](#)[|◀](#)[▶|](#)[Back](#)[Close](#)[Full Screen / Esc](#)[Printer-friendly Version](#)[Interactive Discussion](#)

**Trend analysis of the
Aerosol Optical
Thickness**

J. Yoon et al.

[Title Page](#)[Abstract](#)[Introduction](#)[Conclusions](#)[References](#)[Tables](#)[Figures](#)[|◀](#)[▶|](#)[Back](#)[Close](#)[Full Screen / Esc](#)[Printer-friendly Version](#)[Interactive Discussion](#)

Maenhaut, W., Koren, I. and Holben, B. N.: Dust and pollution aerosols over the Negev desert, Israel: Properties, transport, and radiative effect, *J. Geophys. Res.*, 111, D05205, doi:10.1029/2005JD006549, 2006.

Di Girolamo, L. and Wilson, M. J.: A first look at banddifference angular signatures for cloud detection from MISR, *IEEE Trans. Geosci. Remote Sens.*, 41, 7, 1730–1734, doi:10.1109/TGRS.2003.815659, 2003.

Diner, D. J., Abdou, W. A., Ackerman, T. P., Crean, K., Gordon, H. R., Kahn, R. A., Martonchik, J. V., Paradise, S. R., Pinty, B., Verstraete, M. M., Wang, M., and West, R. A.: Multi-angle Imaging SpectroRadiometer Level 2 Aerosol Retrieval Algorithm Theoretical Basis, Revision F, Jet Propulsion Laboratory, California Institute of Technology JPL D-11400, 2006.

Dubovik, O. and King, M. D.: A flexible inversion algorithm for retrieval of aerosol optical properties from Sun and sky radiance measurements, *J. Geophys. Res.*, 105, 20673–20696, 2000.

Dubovik, O., Smirnov, A., Holben, B. N., King, M. D., Kaufman, Y. J., Eck, T. F. and Slutsker, I.: Accuracy assessment of aerosol optical properties retrieval from AERONET sun and sky radiance measurements, *J. Geophys. Res.*, 105, 9791–9806, 2000.

Dubovik, O., Holben, B. N., Eck, T. F., Smirnov, A., Kaufman, Y. J., King, M. D., Tanré, D., and Slutsker, I.: Variability of absorption and optical properties of key aerosol types observed in worldwide locations, *J. Atmos. Sci.*, 59, 590–608, 2001.

Dubovik, O., Holben, B. N., Lapyonok, T., Sinyuk, A., Mishchenko, M. I., Yang, P. and Slutsker, I.: Non-spherical aerosol retrieval method employing light scattering by spheroids, *Geophys. Res. Lett.*, 10, 1415–1418, doi:10.1029/2001GL014506, 2002.

Dubovik, O., Sinyuk, A., Lapyonok, T., Holben, B. N., Mishchenko, M., Yang, P., Eck, T. F., Volten, H., Munoz, O., Veihelmann, B., van der Zander, W. J., Leon, J. –F., Sorokin, M. and Slutsker, I.: Application of light scattering by spheroids for accounting for particle non-sphericity in remote sensing of desert dust, *J. Geophys. Res.*, 111, D11208, doi:10.1029/2005JD006619, 2006.

Eck, T. F., Holben, B. N., Reid, J. S., Dubovik, O., Smirnov, A., O'Neill, N. T., Slutsker, I., and Kinne, S.: Wavelength dependence of the optical depth of biomass burning, urban, and desert dust aerosol, *J. Geophys. Res.*, 104, 31333–31350, 1999.

Evan, A. T., Mahowald, N. M., and Remer, L. A.: Global Aerosols, *Bull. Am. Meteorol. Soc.*, 88, s1–s135, 2007.

Foster, A. and Kumar, N.: Health effects of air quality regulations in Delhi, India, *Atmos. Envi-*

Trend analysis of the Aerosol Optical Thickness

J. Yoon et al.

[Title Page](#)[Abstract](#)[Introduction](#)[Conclusions](#)[References](#)[Tables](#)[Figures](#)[|◀](#)[▶|](#)[Back](#)[Close](#)[Full Screen / Esc](#)[Printer-friendly Version](#)[Interactive Discussion](#)

ron., 45(9), 1675–1683, 2011.

Garstang, M. and Fitzjarrald, D. R.: Observations of Surface to Atmosphere Interactions in the Tropics, New York, USA, Oxford University Press, 1999.

Gerasopoulos, E., Andreae, M. O., Zerefos, C. S., Andreae, T. W., Balis, D., Formenti, P., Merlet, P., Amiridis, V., and Papastefanou, C.: Climatological aspects of aerosol optical properties in Northern Greece, *Atmos. Chem. Phys.*, 3, 2025–2041, doi:10.5194/acp-3-2025-2003, 2003.

Glen, W. G., Zelenka, M. P., and Graham, R. C.: Relating meteorological variables and trends in motor vehicle emissions to monthly urban carbon monoxide concentrations, *Atmos. Environ.*, 30(24), 4225–4232, 1996.

Gobbi, G. P., Kaufman, Y. J., Koren, I., and Eck, T. F.: Classification of aerosol properties derived from AERONET direct sun data, *Atmos. Chem. Phys.*, 7, 453–458, doi:10.5194/acp-7-453-2007, 2007.

Hao, W. M. and Liu, M.: Spatial and temporal distribution of tropical biomass burning, *Glob. Biogeochem. Cy.*, 8, 495–504, 1994.

Haywood, J. and Boucher, O.: Estimates of the direct and indirect radiative forcing due to tropospheric aerosols: A review, *Review of Geophysics*, 38, 513–543, 2000.

Haywood, J. M., Francis, P. N., Geogdzhayev, I., Mishchenko, M., and Frey, R.: Comparison of Saharan dust aerosol optical depths retrieved using aircraft mounted pyranometers and 2-channel AVHRR algorithms, *Geophys. Res. Lett.*, 28(12), 2393–2396, 2001.

Heidinger, A. K., Goldberg, M. D., Tarpley, D., Jelenak, A., and Pavolonis, M.: A new AVHRR cloud climatology. Applications with Weather Satellites II, Honolulu, Hawaii, 9–11 November 2004. Proceedings, SPIE-The International Society for Optical Engineering, Bellingham, WA, 2005, 197–205, Call Number: Reprint # 4198, 2004.

Higurashi, A. and Nakajima, T.: Development of a two channel aerosol retrieval algorithm on global scale using NOAA AVHRR, *J. Atmos. Sci.*, 56, 924–941, 1999.

Higurashi, A., Nakajima, T., Holben, B. N., Smirnov, A., Frouin, R., and Chatenet, B.: A study of global aerosol optical climatology with two-channel AVHRR remote sensing, *J. Climate*, 13, 12, 2011–2027, doi:10.1175/1520-0442(2000)013<2011:ASOGAO>2.0.CO;2, 2000.

Holben, B. N., Eck, T. F., Slutsker, I., Tanré, D., Buis, J. P., Setzer, A., Vermote, E., Reagan, J. A., Kaufman, Y. J., Nakajima, T., Lavenu, F., Jankowiak, I., and Smirnov, A.: AERONET – A federated instrument network and data archive for aerosol characteristics, *Remote Sens. Environ.*, 66, 1–16, 1998.

Holben, B. N., Tanré, D., Smirnov, A., Eck, T. F., Slutsker, I., Abu Hassan, N., Newcomb, W.

- W., Schafer, J. S., Chatenet, B., Lavenu, F., Kaufman, Y. J., Vande Castle, J., Setzer, A., Markham, B., Clark, D., Frouin, R., Halthore, R., Karneli, A., O'Neill, N. T., Pietras, C., Pinker, R. T., Voss, K., and Zibordi, G.: An emerging ground-based aerosol climatology: Aerosol optical depth from AERONET, *J. Geophys. Res.*, 106, 12067–12097, 2001.
- 5 Huang, J., Zhang, C., and Prospero, J. M.: African aerosol and large-scale precipitation variability over West Africa, *Environ. Res. Lett.*, 4, 015006, doi:10.1088/1748-9326/4/1/015006, 2009.
- Husar, R. B., Prospero, J. M., and Stowe, L. L.: Characterization of tropospheric aerosols over the oceans with the NOAA advanced very high resolution radiometer optical thickness operational product, *J. Geophys. Res.*, 102, D14, 16889–16910, 1997.
- 10 Ignatov, A. and Nalli, N. R.: Aerosol retrievals from the multiyear multisatellite AVHRR pathfinder atmosphere (PATMOS) dataset for correcting remotely sensed sea surface temperatures, *J. Atmos. Oceanic Technol.*, 19(12), 1986–2008, doi:10.1175/1520-0426(2002)019, 2002.
- 15 Ignatov, A. and Stowe, L.: Sensitivity and information content of aerosol retrievals from AVHRR: Radiometric factors, *Appl. Opt.*, 41(6), 991–1011, doi:10.1364/AO.41.000991, 2002.
- IPCC: Changes in Atmospheric Constituents and in Radiative Forcing: Issues Related to Aerosols, 153–179, 2007.
- 20 Jeong, M.-J. and Li, Z.: Quality, compatibility, and synergy analyses of global aerosol products of global aerosol products derived from the advanced very high resolution radiometer and Total Ozone Mapping Spectrometer, *J. Geophys. Res.*, 110, D10S08, doi:10.1029/2004JD004647, 2005.
- Jeong, M.-J., Li, Z., Chu, D. A., and Tsay, S. -T.: Quality and compatibility analyses of global aerosol products derived from the advanced very high resolution radiometers and the moderate imaging spectroradiometer, *J. Geophys. Res.*, 110, D10S09, doi:10.1029/2004JD004648, 2005.
- 25 Kahn, R., Li, W.-H., Martonchik, J., Bruegge, C., Diner, D., Gaitley, B., Abdou, W., Dubovik, O., Holben, B., Smirnov, S., Jin, Z., and Clark, D.: MISR low-light-level calibration, and implications for aerosol retrieval over dark water, *J. Atmos. Sci.*, 62, 4, 1032–1062, doi:10.1175/JAS3390.1, 2005.
- Kahn, R., Garay, M., Nelson, D., Yau, K., Bull, M., and Martonchik, J.: Satellite-derived aerosol optical depth over dark water from MISR and MODIS: Comparisons with AERONET and implications for climatological studies, *J. Geophys. Res.*, 112, D18205,

Trend analysis of the Aerosol Optical Thickness

J. Yoon et al.

[Title Page](#)[Abstract](#)[Introduction](#)[Conclusions](#)[References](#)[Tables](#)[Figures](#)[|◀](#)[▶|](#)[Back](#)[Close](#)[Full Screen / Esc](#)[Printer-friendly Version](#)[Interactive Discussion](#)

doi:10.1029/2006JD008175, 2007.

Kalashnikova, O. V. and Kahn, R.: Ability of multi-angle remote sensing observations to identify and distinguish mineral dust types: Part 2. Sensitivity data analysis, *J. Geophys. Res.*, 111(D11), D11207, doi:10.1029/2005JD006756, 2006.

5 Karnieli, A., Derimian, Y., Indoitu, R., Panov, N., Levy, R. C., Remer, L. A., Maenhaut, W., and Holben, B. N.: Temporal trend in anthropogenic sulfur aerosol transport from central and eastern Europe to Israel, *J. Geophys. Res.*, 114, D00D19, doi:10.1029/2009JD011870, 2009.

Kaufman, Y. J.: Aerosol optical thickness and atmospheric path radiance, *J. Geophys. Res.*, 98(D2), 2677–2692, 1993.

10 Kaufman, Y. J., Tanré, D., Gordon, H. R., Nakajima, T., Lenoble, J., Frouin, R., Grassl, H., Herman, B. M., King, M. D., and Teillet, P. M.: Passive remote sensing of tropospheric aerosol and atmospheric correction for the aerosol effect, *J. Geophys. Res.*, 102, 16815–16830, 1997.

15 Kim, S.-W., Yoon, S.-C., Kim, J., and Kim, S.-Y.: Seasonal and monthly variations of columnar aerosol optical properties over East Asia determined from multi-year MODIS, LIDAR, and AERONET sun/sky radiometer measurements, *Atmos. Environ.*, 41, 1634–1651, 2007.

Kokhanovsky, A. and de Leeuw, G.: Satellite aerosol remote sensing over land, Springer, 2009.

Kotchenruther, R., Hobbs, P. V., and Hegg, D. A.: Humidification factors for atmospheric aerosols off the mid-Atlantic coast of the United States, *J. Geophys. Res.*, 104, 2239–2251, 1999.

20 Kubilay, N., Cokacar, T., and Oguz, T.: Optical properties of mineral dust outbreaks over the northeastern Mediterranean, *J. Geophys. Res.*, 108(D21), 4666, doi:10.1029/2003JD003798, 2003.

25 Léon, J.-F., Chazette, P., Dulac, F., Pelon, J., Bonnazola, M., Foret, G., Cautenet, S., Cachier, C., Alfaro, S. C., Gaudichet, A., Gomes, L., Rajot, J.-L., Lavenu, F., Inamdar, S. R., and Sarode, P. R.: Large scale advection of continental aerosols during INDOEX, *J. Geophys. Res.*, 106, D22, 28427–28439, 2001.

30 Li, Z., Zhao, X., Kahn, R., Mishchenko, M., Remer, L., Lee, K.-H., Wang, M., Laszlo, I., Nakajima, T., and Maring, H.: Uncertainties in satellite remote sensing of aerosols and impact on monitoring its long-term trend: a review and perspective, *Ann. Geophys.*, 27, 2755–2770, 2009,
<http://www.ann-geophys.net/27/2755/2009/>.

Liu, Y., Sarnat, J. A., Coull, B. A., Koutrakis, P., and Jacob, D. J.: Validation of Multiangle Imaging Spectroradiometer (MISR) aerosol optical thickness measurements using Aerosol

AMTD

4, 5325–5388, 2011

Trend analysis of the Aerosol Optical Thickness

J. Yoon et al.

Title Page

Abstract

Introduction

Conclusions

References

Tables

Figures

◀

▶

Back

Close

Full Screen / Esc

Printer-friendly Version

Interactive Discussion



**Trend analysis of the
Aerosol Optical
Thickness**

J. Yoon et al.

[Title Page](#)[Abstract](#)[Introduction](#)[Conclusions](#)[References](#)[Tables](#)[Figures](#)[|◀](#)[▶|](#)[◀](#)[▶](#)[Back](#)[Close](#)[Full Screen / Esc](#)[Printer-friendly Version](#)[Interactive Discussion](#)

- Robotic Network (AERONET) observations over the contiguous United States, *J. Geophys. Res.*, 109, D06205, doi:10.1029/2003JD003981, 2004.
- Marmer, E., Langmann, B., Fagerli, H., and Vestreng, V.: Direct shortwave radiative forcing of sulphate aerosol over Europe from 1900 to 2000, *J. Geophys. Res.*, 112, D23S17, doi:10.1029/2006JD008037, 2007.
- Martins, J. V., Remer, L., Kaufman, Y. J., Mattoo, S., and Levy, R.: MODIS cloud screening for remote sensing of aerosols over oceans using spatial variability, *Geophys. Res. Lett.*, 29(12), 8009, doi:10.1029/2001GL013252, 2002.
- Martonchik, J. V., Diner, D. J., Kahn, R. A., Gaitley, B. J., and Holben, B. N.: Comparison of MISR and AERONET aerosol optical depths over desert sites, *Geophys. Res. Lett.*, 31, L16101, doi:10.1029/2004GL019807, 2004.
- Massie, T. S., Torres, O., and Smith, S. J.: Total ozone mapping spectrometer (TOMS) observations of increases in Asian aerosol in winter from 1979 to 2000, *J. Geophys. Res.*, 109, D18211, doi:10.1029/2004JD004620, 2004.
- Mishchenko, M. and Geogdzhayev, I. V.: Satellite remote sensing reveals regional tropospheric aerosol trends, *Opt. Express*, 15(12), 7423–7438, 2007.
- Mishchenko, M. I., Geogdzhayev, I. V., Cairns, B., Rossow, W. B., and Lacis, A. A.: Aerosol retrievals over the ocean by use of channels 1 and 2 AVHRR data: sensitivity analysis and preliminary results, *Appl. Opt.*, 38, 7325–7341, 1999a.
- Mishchenko, M. I., Dlugach, J. M., Yanovitskij, E. G., and Zakharova, N. T.: Bidirectional reflectance of flat, optically thick particulate layers: an efficient radiative transfer solution and applications to snow and soil surfaces, *J. Quant. Spectrosc. Radiat. Transfer*, 63, 409–432, 1999b.
- Mishchenko, M. I., Travis, L. D., and Lacis, A. A.: Scattering, Absorption, and Emission of Light by Small Particles, Cambridge University Press, 2002.
- Mishchenko, M., Geogdzhayev, I. V., Rossow, W. B., Cairns, B., Carlson, B. E., Lacis, A. A., Liu, L., and Travis, L. D.: Long-term satellite record reveals likely recent aerosol trend, *Science*, 315, p. 1543, 2007.
- Moulin, C. and Chiapello, I.: Evidence of the control of summer atmospheric transport of African dust over the Atlantic by Sahel sources from TOMS satellites (1979–2000), *Geophys. Res. Lett.*, 31, L02107, doi:10.1029/2003GL018931, 2004.
- Mukai, S., Sano, I., and Holben, B. N.: Aerosol properties over Japan by sun/sky photometry, *Water Air Soil Pollut.*, 5, 133–143, 2005.

Trend analysis of the Aerosol Optical Thickness

J. Yoon et al.

[Title Page](#)

[Abstract](#)

[Introduction](#)

[Conclusions](#)

[References](#)

[Tables](#)

[Figures](#)

◀

▶

[Back](#)

[Close](#)

[Full Screen / Esc](#)

[Printer-friendly Version](#)

[Interactive Discussion](#)



- Mukai, S., Sano, I., Satoh, M., and Holben, B. N.: Aerosol properties and air pollutants over an urban area, *Atmos. Res.*, 82, 643–651, 2006.
- Myhre, G., Stordal, F., Johnsrud, M., Ignatov, A., Mishchenko, M. I., Geogdzhayev, I. V., Tanré, D., Deuz'e, J.-L., Goloub, P., Nakajima, T., Higurashi, A., Torres, O., and Holben, B. N.: Intercomparison of satellite retrieved aerosol optical depth over the ocean, *J. Atmos. Sci.*, 61(5), 499–513, doi:10.1175/1520-0469(2004)061, 2004.
- Norris, J. R. and Wild, M.: Trends in aerosol radiative effects over Europe inferred from observed cloud cover, solar “dimming,” and solar “brightening”, *J. Geophys. Res.*, 112, D08214, doi:10.1029/2006JD007794, 2007.
- Ohmura, A.: Observed long-term variations of solar irradiance at the Earth's surface, *Space Sci. Rev.*, 125, 111–128, 2006.
- O'Neill, N. T., Dubovik, O., and Eck, T. F.: A modified Angstrom coefficient for the characterization of sub-micron aerosols, *Appl. Opt.*, 40, 2368–2375, 2001a.
- O'Neill, N. T., Eck, T. F., Holben, B. N., Smirnov, A., and Dubovick, O.: Bimodal size distribution influences on the variation of Angstrom derivatives in spectral and optical depth space, *J. Geophys. Res.*, 106(D9), 9787–9806, 2001b.
- O'Neill, N. T., Eck, T. F., Smirnov, A., Holben, B. N., and Thulasiraman, S.: Spectral discrimination of coarse and fine mode optical depth, *J. Geophys. Res.*, 108(D17), 4559, doi:10.1029/2002JD002975, 2003.
- O'Neill, N. T., Thulasiraman, S., Eck, T. F., and Reid, J.S.: Robust optical features of fine mode size distributions: Application to the Quebec smoke event of 2002, *J. Geophys. Res.*, 110, D11207, doi:10.1029/2004JD005157, 2005.
- Ortore, E. and Francione, V.: On the aerosols monitoring by satellite observations, *Clean Technol. Environ. Policy*, 10(2), 137, doi:10.1007/s10098-007-0134-3, 2008.
- Penner, J. E., Andreae, M., Annegarn, H., Barrie, L., Feichter, J., Hegg, D., Jayaraman, A., Leaitch, R., Murphy, D., Nganga, J., and Pitari, G.: Aerosols, their Direct and Indirect Effects, in Climate Change, Report to Intergovernmental Panel on Climate Change from the Scientific Assessment Working Group (WGI), Cambridge University Press, 289–416, 2001.
- Pereira, S. N., Wagner, F., and Silva, A. M.: Seven years of measurements of aerosol scattering properties, near the surface, in the southwestern Iberia Peninsula, *Atmos. Chem. Phys.*, 11, 17–29, doi:10.5194/acp-11-17-2011, 2011.
- Prospero, J. M. and Lamb, J. P.: African droughts and dust transport to the Caribbean: climate change and implications, *Science*, 302, 1024–1027, 2003.

Ramanathan, V., Crutzen, P. J., Lelieveld, J., Mitra, A. P., Althausen, D., Andersons, J., Andreae, M. O., Cantrell, W., Cass, G. R., Chung, C. E., Clarke, A. D., Coakley, J. A., Collins, W. D., Conant, W. C., Dulac, F., Heintzenberg, J., Heymsfield, A. J., Holben, B., Howell, S., Hudson, J., Jayaraman, A., Kiehl, J. T., Krishnamurti, T. N., Lubin, D., McFarquhar, G., Novakov, T., Ogren, J. A., Podgorny, I. A., Prather, K., Priestley, K., Prospero, J. M., Quinn, P. K., Rajeev, K., Rasch, P., Rupert, S., Sadourny, R., Satheesh, S. K., Shaw, G. E., Sheridan, P., and Valero, F. P. J.: Indian Ocean experiment: An integrated analysis of the climate forcing and effects of the great Indo-Asian haze, *J. Geophys. Res.*, 106, D22, 28371–28398, 2001.

Reeves, C. E., Formenti, P., Afif, C., Ancellet, G., Attié, J.-L., Bechara, J., Borbon, A., Cairo, F., Coe, H., Crumeyrolle, S., Fierli, F., Flamant, C., Gomes, L., Hamburger, T., Jambert, C., Law, K. S., Mari, C., Jones, R. L., Matsuki, A., Mead, M. I., Methven, J., Mills, G. P., Minikin, A., Murphy, J. G., Nielsen, J. K., Oram, D. E., Parker, D. J., Richter, A., Schlager, H., Schwarzenboeck, A., and Thouret, V.: Chemical and aerosol characterisation of the troposphere over West Africa during the monsoon period as part of AMMA, *Atmos. Chem. Phys.*, 10, 7575–7601, doi:10.5194/acp-10-7575-2010, 2010.

Remer, L. A., Gasso, S., Hegg, D. A., Kaufman, Y. J., and Holben, B. N.: Urban/industrial aerosol: Ground-based sun/sky radiometer and airborne in situ measurements, *J. Geophys. Res.*, 102, 16849–16859, 1997.

Remer, L. A., Kaufman, Y. J., Tanré, D., Mattoo, S., Chu, D. A., Martins, J. V., Li, R. –R., Ichoku, C., Levy, R. C., Kleidman, R. G., Eck, T. F., Vermote, E., and Holben, B. N.: The MODIS Aerosol Algorithm, Products, and Validation, *J. Atmos. Sci.*, 62, 947–973, 2005.

Robles González C., Veefkind, J. P., and de Leeuw, G.: Aerosol optical depth over Europe in August 1997 derived from ATSR-2 data, *Geophys. Res. Lett.*, 27(7), 955–958, 2000.

Sabbah, I. and Hasan, F. M.: Remote sensing of aerosols over the Solar Village, Saudi Arabia, *Atmos. Res.*, 90, 170–179, 2008.

Sabbah, I., Ichoku, C., Kaufman, Y. J., and Remer, L.: Full year cycle of desert dust spectral optical thickness and precipitable water vapour over Alexandria, Egypt, *J. Geophys. Res.*, 106, 18305–18316, 2001.

Sabbah, I., Saeed, T., Al Jassar, H. K., and Rao, K. S.: Remote sensing of desert dust in Kuwait, *J. Sci. Eng.* 33, 101–117, 2006.

Sano, I., Mukai, S., Okada, Y., Holben, B. N., Ohta, S., and Takamura, T.: Optical properties of aerosols during APEX and ACE-Asia experiments, *J. Geophys. Res.*, 108, 8649, doi:10.1029/2002JD003263, 2003.

Trend analysis of the Aerosol Optical Thickness

J. Yoon et al.

[Title Page](#)

[Abstract](#)

[Introduction](#)

[Conclusions](#)

[References](#)

[Tables](#)

[Figures](#)

[◀](#)

[▶](#)

[Back](#)

[Close](#)

[Full Screen / Esc](#)

[Printer-friendly Version](#)

[Interactive Discussion](#)



Trend analysis of the Aerosol Optical Thickness

J. Yoon et al.

- Schmeissner, T., Krejci, R., Ström, J., Birmili, W., Wiedensohler, A., Hochschild, G., Gross, J., Hoffmann, P., and Calderon, S.: Analysis of number size distributions of tropical free tropospheric aerosol particles observed at Pico Espejo (4765 m a.s.l.), Venezuela, *Atmos. Chem. Phys.*, 11, 3319–3332, doi:10.5194/acp-11-3319-2011, 2011.
- 5 Schuster, G. L., Dubovik, O., and Holben, B. N.: Angstrom exponent and bimodal aerosol size distributions, *J. Geophys. Res.*, 111, D07207, doi:10.1029/2005JD006328, 2006.
- Shinozuka, Y., Redemann, J., Livingston, J. M., Russell, P. B., Clarke, A. D., Howell, S. G., Freitag, S., O'Neill, N. T., Reid, E. A., Johnson, R., Ramachandran, S., McNaughton, C. S., Kapustin, V. N., Brekhovskikh, V., Holben, B. N., and McArthur, L. J. B.: Airborne observation 10 of aerosol optical depth during ARCTAS: vertical profiles, inter-comparison and fine-mode fraction, *Atmos. Chem. Phys.*, 11, 3673–3688, doi:10.5194/acp-11-3673-2011, 2011.
- 15 Sinyuk, A., Dubovik, O., Holben, B. N., Eck, T. F., Breon, F. -M., Martonchik, J., Kahn, R., Diner, D. J., Vermote, E. F., Roger, J. -C., Lapyonok, T., and Slutsker, I.: Simultaneous retrieval of aerosol and surface properties from a combination of AERONET and satellite data, *Remote Sens. of Environ.*, 107, 90–108, 2007.
- 20 Smirnov, A., Holben, B. N., Eck, T. F., Dubovik, O., and Slutsker, I.: Cloud screening and quality control algorithms for the AERONET data base, *Rem. Sens. Env.*, 73(3), 337–349, 2000.
- Smirnov, A., Holben, B.N., Dubovik, O., Neil, N., and Eck, T.F.: Atmospheric aerosol optical 25 properties in the Persian Gulf, *Atmos. Sci.*, 59, 620–634, 2002.
- Smith, S. J., Pitcher, H., and Wigley, T. M. L.: Global and regional anthropogenic sulfur dioxide emissions, *Global Planet. Change*, 29, 99–119, 2001.
- Smith, S. J., Andres, R., Conception, E., and Lurz, J.: Historical sulfur dioxide emissions 1850–2000: Methods and results, *PNNL Res. Rep.* 14537, Pac. Northwest Natl. Lab., Richland, Wash, 2003.
- 30 Stanhill, G.: A perspective on global warming, dimming, and brightening, *EOS Trans. Amer. Geophys. Union*, 88, 58, 2007.
- Stowe, L. L., Davis, P. A., and McClain, E. P.: Scientific basis and initial evaluation 35 of the CLAVR-1 global clear/cloud classification algorithm for the Advanced Very High Resolution Radiometer, *J. Atmos. Oceanic Technol.*, 16(6), 656–681, doi:10.1175/1520-0426(1999)016<0656:SBAIEO>2.0.CO;2, 1999.
- Streets, D. G., Tsai, N. Y., Akimoto, H., and Oka, K.: Sulfur dioxide emissions in Asia in the period 1985–1997, *Atmos. Environ.*, 34, 4413–4424, 2000.
- Streets, D. G., Bond, T. C., Carmichael, G. R., Fernandes, S. D., Fu, Q., He, D., Klimont, Z., Nel-

[Title Page](#)[Abstract](#)[Introduction](#)[Conclusions](#)[References](#)[Tables](#)[Figures](#)[◀](#)[▶](#)[Back](#)[Close](#)[Full Screen / Esc](#)[Printer-friendly Version](#)[Interactive Discussion](#)

**Trend analysis of the
Aerosol Optical
Thickness**

J. Yoon et al.

son, S. M., Tsai, N. Y., Wang, M. Q., Woo, J. -H., and Yarber, K. F.: An inventory of gaseous and primary aerosol emissions in Asia in the year 2000, *J. Geophys. Res.*, 108(D21), 8809, doi:10.1029/2002JD003093, 2003.

Streets, D. G., Wu, Y., and Chin, M.: Two-decadal aerosol trends as a likely explanation of the global dimming/brightening transition, *Geophys. Res. Lett.*, 33, L15806, doi:10.1029/2006GL026471, 2006.

Streets, D. G., Yan, F., Chin, M., Diehl, T., Mahowald, N., Schultz, M., Wild, M., Wu, Y., and Yu, C.: Anthropogenic and natural contributions to regional trends in aerosol optical depth, 1980–2006, *J. Geophys. Res.*, 114, D00D18, doi:10.1029/2008JD011624, 2009.

Swap, R., Garstang, M., Macko, S. A., Tyson, P. D., Maenhaut, W., Artaxo, P., Källberg, P. and Talbot, R.: The long-range transport of southern African aerosols to the tropical South Atlantic, *J. Geophys. Res.*, 101(D19), 23777–23791, 1996.

Tafuro, A. M., Barnaba, F., De Tomasi, F., Perrone, M. R., and Gobbi, G. P.: Saharan dust particle properties over the central Mediterranean, *Atmos. Res.*, 81, 67–93, 2006.

Tanré, D., Bréon, F. M., Deuzé, J. L., Herman, M., Goloub, P., Nadal, F., and Marchand, A.: Global observation of anthropogenic aerosols from satellite, *Geophys. Res. Lett.*, 28(24), 4555–4558, 2001.

Torres, O., Bhartia, P. K., Herman, J. R., Sinyuk, A. and Holben, B.: A long term record of aerosol optical thickness from TOMS observations and comparison to AERONET measurements, *J. Atm. Sci.*, 59, 398–413, 2002.

Tyson, P. D.: Climatic Change and Variability in Southern Africa, Oxford Univ. Press, 220, 1986.

Venzac, H., Sellegri, K., Villani, P., Picard, D., and Laj, P.: Seasonal variation of aerosol size distributions in the free troposphere and residual layer at the puy de Dôme station, France, *Atmos. Chem. Phys.*, 9, 1465–1478, doi:10.5194/acp-9-1465-2009, 2009.

von Hoyningen-Huene, W., Yoon, J., Vountas, M., Istomina, L. G., Rohen, G., Dinter, T., Kokhanovsky, A. A., and Burrows, J. P.: Retrieval of spectral aerosol optical thickness over land using ocean colour sensors MERIS and SeaWiFS, *Atmos. Meas. Tech.*, 4, 151–171, doi:10.5194/amt-4-151-2011, 2011.

Washington, R. and Todd, M. C.: Atmospheric controls on mineral dust emission from the Bodélé depression, chad: the role of the low level jet, *Geophys. Res. Lett.*, 32, L17701, doi:10.1029/2005GL023597, 2005.

Wild, M., Gilgen, H., Roesch, A., Ohmura, A., Long, C. N., Dutton, E. G., Forgan, B., Kallis, A., Russak, V., and Tsvetkov, A.: From dimming to brightening: Decadal changes in solar

[Title Page](#)[Abstract](#)[Introduction](#)[Conclusions](#)[References](#)[Tables](#)[Figures](#)[|◀](#)[▶|](#)[Back](#)[Close](#)[Full Screen / Esc](#)[Printer-friendly Version](#)[Interactive Discussion](#)

**Trend analysis of the
Aerosol Optical
Thickness**

J. Yoon et al.

[Title Page](#)[Abstract](#)[Introduction](#)[Conclusions](#)[References](#)[Tables](#)[Figures](#)[|◀](#)[▶|](#)[◀](#)[▶|](#)[Back](#)[Close](#)[Full Screen / Esc](#)[Printer-friendly Version](#)[Interactive Discussion](#)

Trend analysis of the Aerosol Optical Thickness

J. Yoon et al.

Table 1. Geolocations and research periods of the suitable AERONET stations for aerosol trend analysis in alphabetical order.

Selected AERONET Stations	Regions	Countries	Geolocations (lat.[°]/lon.[°]/ alt.[m])	Research Periods
(a) Avignon	Western Europe	France	43.93/4.88/32	2001~2005
(b) Banizoumbou	West Africa	Niger	13.54/2.66/250	2002 ~ 2008
(c) Beijing	East Asia	China	39.98/116.38/92	2003 ~ 2007
(d) Dakar	West Africa	Senegal	14.39/-16.96/0	2004 ~ 2008
(e) GSFC	North America	USA	38.99/-76.84/87	1995 ~ 2008
(f) Ispra	Western Europe	Italy	45.80/8.63/235	2001 ~ 2007
(g) Mauna_Loa	Free troposphere (Pacific)	USA	19.54/-155.58/3397	1998 ~ 2009
(h) MD_Science_Center	North America	USA	39.28/-76.62/15	2000 ~ 2006
(i) Mongu	South Africa	Zambia	-15.25/23.15/1107	2000 ~ 2004
(j) Ouagadougou	West Africa	Burkina Faso	12.20/-1.40/290	2000 ~ 2004
(k) SEDE_BOKER	Middle East	Israel	30.86/34.78/480	2003 ~ 2008
(l) Sevilleta	North America	USA	34.35/-106.89/1477	1998 ~ 2002
(m) Shirahama	East Asia	Japan	33.69/135.36/10	2003 ~ 2009
(n) Skukuza	South Africa	South Africa	-24.99/31.59/150	2000 ~ 2007
(o) Solar_Village	Middle East	Saudi Arabia	24.91/46.40/764	2001 ~ 2007



Trend analysis of the Aerosol Optical Thickness

J. Yoon et al.

Table 2. Bimodal lognormal volume size distribution ($\frac{dV(r)}{d\ln r}$) parameters and refractive indices (Schuster et al., 2006) used to compute ÅE (440–870 nm) and ÅED (ÅE(440–675 nm)–ÅE(675–870 nm)) using Mie code in Fig. 4.

Parameter*	Values
r_{fine}	0.06, 0.09, 0.12, 0.15, 0.18, 0.21, 0.24, 0.27, 0.30
σ_{fine}	0.38, 0.50
r_{coarse}	1.9, 2.2, 2.7, 2.8, 3.0, 3.2, 3.4, 3.6, 3.7
σ_{coarse}	0.75, 1.00
n	1.34, 1.37, 1.40, 1.43, 1.47, 1.50, 1.54
k	0.003
$C_{\text{fine}}/C_{\text{total}}$	0.01, 0.10, 0.20, 0.30, 0.40, 0.50, 0.60, 0.70, 0.80, 0.90, 0.99

* The bimodal lognormal volume size distribution ($\frac{dV(r)}{d\ln r}$) is given by

$$\frac{dV(r)}{d\ln r} = \frac{C_{\text{fine}}}{\sqrt{2\pi}\sigma_{\text{fine}}} \exp\left[-\frac{(\ln r - \ln r_{\text{fine}})^2}{2\sigma_{\text{fine}}^2}\right] + \frac{C_{\text{coarse}}}{\sqrt{2\pi}\sigma_{\text{coarse}}} \exp\left[-\frac{(\ln r - \ln r_{\text{coarse}})^2}{2\sigma_{\text{coarse}}^2}\right],$$

where $C_{\text{total,fine,coarse}}$ represents the particle volume concentration for total, fine and coarse aerosol modes [$\mu\text{m}^3/\mu\text{m}^2$], $r_{\text{fine,coarse}}$ is the median or geometric mean radius [μm], and $\sigma_{\text{fine,coarse}}$ is the variance or width of each mode. n and k represent the real and imaginary parts of the complex refractive index, respectively.

[Title Page](#)
[Abstract](#) [Introduction](#)
[Conclusions](#) [References](#)
[Tables](#) [Figures](#)

[|◀](#) [▶|](#)

[◀](#) [▶](#)
[Back](#) [Close](#)

[Full Screen / Esc](#)

[Printer-friendly Version](#)
[Interactive Discussion](#)



Trend analysis of the Aerosol Optical Thickness

J. Yoon et al.

[Title Page](#)

[Abstract](#)

[Introduction](#)

[Conclusions](#)

[References](#)

[Tables](#)

[Figures](#)

◀

▶

◀

▶

[Back](#)

[Close](#)

[Full Screen / Esc](#)

[Printer-friendly Version](#)

[Interactive Discussion](#)



Table 3. Summary of aerosol optical properties for urban-industrial and mixed, biomass burning, desert dust, and oceanic types from Dubovik et al (2001) based on worldwide AERONET of ground-based radiometers. These properties are used to compute ÅE (440–870 nm) and ÅED ($\text{ÅE}(440\text{--}675 \text{ nm}) - \text{ÅE}(675\text{--}870 \text{ nm})$) using Mie code and depicted by solid, dotted, dashed, dash-dot-dot lines sequentially in Fig. 5.

Urban-industrial and mixed	GSFC, Greenbelt, MD (1993–2000)	Crete-Paris, France (1999)
Range of optical thickness; $\langle \tau \rangle^*$	$0.1 \leq \tau(440) \leq 1.0$; 0.24	$0.1 \leq \tau(440) \leq 0.9$; 0.26
Refractive indices(n ; k)	$1.41 - 0.03\tau(440)$; 0.003	1.40; 0.009
$r_{\text{fine}} [\mu\text{m}]$; σ_{fine}	$0.12 + 0.11\tau(440)$; 0.38	$0.11 + 0.13\tau(440)$; 0.43
$r_{\text{coarse}} [\mu\text{m}]$; σ_{coarse}	$3.03 + 0.49\tau(440)$; 0.75	$2.76 + 0.48\tau(440)$; 0.79
$C_{\text{fine}} [\mu\text{m}^3/\mu\text{m}^2]$	$0.15\tau(440)$	$0.01 + 0.12\tau(440)$
$C_{\text{coarse}} [\mu\text{m}^3/\mu\text{m}^2]$	$0.01 + 0.04\tau(440)$	$0.01 + 0.05\tau(440)$
Mexico City Maldives (INDOEX) (1999–2000)		
		(1999–2000)
Range of optical thickness; $\langle \tau \rangle$	$0.1 \leq \tau(440) \leq 1.8$; 0.43	$0.1 \leq \tau(440) \leq 0.7$; 0.27
Refractive indices(n ; k)	1.47; 0.014	1.44; 0.007
$r_{\text{fine}} [\mu\text{m}]$; σ_{fine}	$0.12 + 0.04\tau(440)$; 0.43	0.18; 0.46
$r_{\text{coarse}} [\mu\text{m}]$; σ_{coarse}	$2.72 + 0.60\tau(440)$; 0.63	$2.62 + 0.61\tau(440)$; 0.76
$C_{\text{fine}} [\mu\text{m}^3/\mu\text{m}^2]$	$0.12\tau(440)$	$0.12\tau(440)$
$C_{\text{coarse}} [\mu\text{m}^3/\mu\text{m}^2]$	$0.11\tau(440)$	$0.15\tau(440)$

* $\langle \tau \rangle$ is the average value of Aerosol Optical Thickness (AOT) at λ nm ($\tau(\lambda)$).

Table 3. Continued.

	Amazonian forest, Brazil (1993–1994); Bolivia (1998–1999)	South American cerrado, Brazil (1993–1995)
Biomass burning		
Range of optical thickness; $\langle \tau \rangle^*$	$0.1 \leq \tau(440) \leq 3.0$; 0.74	$0.1 \leq \tau(440) \leq 2.1$; 0.80
Refractive indices(n ; k)	1.47; 0.00093	1.52; 0.015
$r_{\text{fine}} [\mu\text{m}]$; σ_{fine}	$0.14+0.13 \tau(440)$; 0.40	$0.14+0.01 \tau(440)$; 0.47
$r_{\text{coarse}} [\mu\text{m}]$; σ_{coarse}	$3.27+0.58 \tau(440)$; 0.79	$3.27+0.51 \tau(440)$; 0.79
$C_{\text{fine}} [\mu\text{m}^3/\mu\text{m}^2]$	$0.12\tau(440)$	$0.1\tau(440)$
$C_{\text{coarse}} [\mu\text{m}^3/\mu\text{m}^2]$	$0.05\tau(440)$	$0.04+0.03 \tau(440)$
		Boreal forest, United States and Canada (1994–1998)
African savanna, Zambia (1995–2000)		
Range of optical thickness; $\langle \tau \rangle$	$0.1 \leq \tau(440) \leq 1.5$; 0.38	$0.1 \leq \tau(440) \leq 2.0$; 0.40
Refractive indices(n ; k)	1.51; 0.021	1.50; 0.0094
$r_{\text{fine}} [\mu\text{m}]$; σ_{fine}	$0.12+0.025 \tau(440)$; 0.40	$0.15+0.015 \tau(440)$; 0.43
$r_{\text{coarse}} [\mu\text{m}]$; σ_{coarse}	$3.22+0.71 \tau(440)$; 0.73	$3.21+0.2 \tau(440)$; 0.81
$C_{\text{fine}} [\mu\text{m}^3/\mu\text{m}^2]$	$0.12\tau(440)$	$0.01+0.1 \tau(440)$
$C_{\text{coarse}} [\mu\text{m}^3/\mu\text{m}^2]$	$0.09\tau(440)$	$0.01+0.03 \tau(440)$

Trend analysis of the Aerosol Optical Thickness

J. Yoon et al.

[Title Page](#)[Abstract](#)[Introduction](#)[Conclusions](#)[References](#)[Tables](#)[Figures](#)[|◀](#)[▶|](#)[◀](#)[▶](#)[Back](#)[Close](#)[Full Screen / Esc](#)[Printer-friendly Version](#)[Interactive Discussion](#)

Table 3. Continued.

Desert dust and oceanic	Bahrain-Persian Gulf (1998–2000)	Solar-Vil.-Saudi Arabia (1998–2000)
Range of optical thickness; $\langle \tau \rangle^*$	$0.1 \leq \tau(1020) \leq 1.2$; 0.22	$0.1 \leq \tau(1020) \leq 1.5$; 0.17
Refractive indices(n)	1.55	1.56
Refractive indices($k(440/670/870/1020\text{ nm})$)	0.0025/0.0014/0.001/0.001	0.0029/0.0013/0.001/0.001
$r_{\text{fine}}[\mu\text{m}]$; σ_{fine}	0.15; 0.42	0.12; 0.40
$r_{\text{coarse}}[\mu\text{m}]$; σ_{coarse}	2.54; 0.61	2.32; 0.60
$C_{\text{fine}}[\mu\text{m}^3/\mu\text{m}^2]$	$0.02 + 0.1 \tau(1020)$	$0.02 + 0.02 \tau(1020)$
$C_{\text{coarse}}[\mu\text{m}^3/\mu\text{m}^2]$	$-0.02 + 0.92 \tau(1020)$	$-0.02 + 0.98 \tau(1020)$
	Cape Verde (1993–2000)	Lanai, HI (1995–2000)
Range of optical thickness; $\langle \tau \rangle$	$0.1 \leq \tau(1020) \leq 2.0$; 0.39	$0.01 \leq \tau(1020) \leq 0.2$; 0.04
Refractive indices(n)	1.48	1.36
Refractive indices($k(440/670/870/1020\text{ nm})$)	0.0025/0.0007/0.0006/0.0006	0.0015
$r_{\text{fine}}[\mu\text{m}]$; σ_{fine}	0.12; $0.49 + 0.10 \tau(1020)$	0.16; 0.48
$r_{\text{coarse}}[\mu\text{m}]$; σ_{coarse}	1.90; $0.63 - 0.10 \tau(1020)$	2.70; 0.68
$C_{\text{fine}}[\mu\text{m}^3/\mu\text{m}^2]$	$0.02 + 0.02 \tau(1020)$	$0.40 \tau(1020)$
$C_{\text{coarse}}[\mu\text{m}^3/\mu\text{m}^2]$	$0.9 \tau(1020)$	$0.80 \tau(1020)$

Trend analysis of the Aerosol Optical Thickness

J. Yoon et al.

[Title Page](#)[Abstract](#)[Introduction](#)[Conclusions](#)[References](#)[Tables](#)[Figures](#)[|◀](#)[▶|](#)[◀](#)[▶](#)[Back](#)[Close](#)[Full Screen / Esc](#)[Printer-friendly Version](#)[Interactive Discussion](#)

Trend analysis of the Aerosol Optical Thickness

J. Yoon et al.

Table 4. Climatological averages, and statistical parameters for weighted and unweighted trend of Ångström Exponent (440–870 nm) and AOTs (440, 675, 870, and 1020 nm) at (a) Avignon, (b) Banizoumbou, (c) Beijing, (d) Dakar, (e) GSFC, (f) Ispra, (g) Mauna_Loa, (h) MD_Science_Center, (i) Mongu, (j) Ouagadougou, (k) SEDE_BOKER, (l) Sevilleta, (m) Shirahama, (n) Skukuza, and (o) Solar_Village.

(a) Avignon			(b) Banizoumbou		
	< τ > ^a	Unweighted trend/[year]		< τ >	Unweighted trend/[year]
		Weighted trend/[year]			Weighted trend/[year]
α^b	1.43	+0.02242(+1.57%)	+0.01364(+0.95%)	0.37	-0.00777(-2.08%)
τ_{440}^c	0.20	+0.00020(+0.10%)	+0.00194(+0.98%)	0.52	-0.00166(-0.32%)
τ_{675}	0.11	-0.00024(-0.22%)	+0.00037(+0.34%)	0.47	+0.00038(+0.08%)
τ_{870}	0.08	-0.00066(-0.85%)	-0.00079(-1.02%)	0.43	+0.00119(+0.28%)
τ_{1020}	0.06	+0.00021(+0.33%)	-0.00035(-0.55%)	0.41	+0.00056(+0.14%)
(c) Beijing			(d) Dakar		
α	1.12	-0.02200(-1.97%)	-0.02308(-2.07%)	0.36	-0.01415(-3.95%)
τ_{440}	0.68	+0.00717(+1.06%)	+0.03100(+4.59%)	0.46	-0.01186(-2.60%)
τ_{675}	0.43	+0.00636(+1.48%)	+0.02448(+5.71%)	0.41	-0.00938(-2.31%)
τ_{870}	0.32	+0.00665(+2.06%)	+0.02023(+6.26%)	0.38	-0.00697(-1.86%)
τ_{1020}	0.27	+0.00673(+2.46%)	+0.01706(+6.25%)	0.36	-0.00649(-1.83%)

$\langle \tau \rangle^a$: Average of Aerosol Optical Thickness at λ nm (τ_λ).

α^b : Ångström Exponent (440–870 nm).

τ_λ^c : AOTs at wavelengths, λ (440, 675, 870, and 1020 nm).

Title Page	
Abstract	Introduction
Conclusions	References
Tables	Figures

◀	▶
◀	▶
Back	Close

Full Screen / Esc
Printer-friendly Version
Interactive Discussion



Trend analysis of the Aerosol Optical Thickness

J. Yoon et al.

Table 4. Continued.

(e) GSFC			(f) Ispra			
	$\langle \tau \rangle^a$	Unweighted trend/[year]	Weighted trend/[year]	$\langle \tau \rangle$	Unweighted trend/[year]	Weighted trend/[year]
α^b	1.59	+0.00816(+0.51%)	+0.00442(+0.28%)	1.51	-0.00038(-0.03%)	-0.00178(-0.12%)
τ_{440}^c	0.22	-0.00085(-0.38%)	-0.00122(-0.54%)	0.30	-0.00337(-1.13%)	-0.00687(-2.30%)
τ_{675}^c	0.11	-0.00095(-0.85%)	-0.00074(-0.67%)	0.16	-0.00206(-1.26%)	-0.00418(-2.57%)
τ_{870}^c	0.07	-0.00080(-1.07%)	-0.00037(-0.50%)	0.11	-0.00101(-0.90%)	-0.00262(-2.34%)
τ_{1020}^c	0.06	-0.00062(-1.05%)	-0.00020(-0.34%)	0.09	-0.00094(-1.06%)	-0.00266(-2.99%)
(g) Mauna_Loa			(h) MD_Science_Center			
α	1.21	+0.01180(+0.97%)	+0.01504(+1.24%)	1.68	-0.01228(-0.73%)	-0.01480(-0.88%)
τ_{440}	0.02	+0.00026(+1.36%)	+0.00033(+1.73%)	0.24	-0.00177(-0.74%)	-0.00003(-0.01%)
τ_{675}	0.01	+0.00003(+0.39%)	+0.00009(+1.11%)	0.12	-0.00089(-0.75%)	-0.00049(-0.41%)
τ_{870}	0.01	+0.00004(+0.46%)	+0.00014(+1.41%)	0.08	-0.00020(-0.26%)	+0.00010(+0.13%)
τ_{1020}	0.01	+0.00003(+0.28%)	+0.00008(+0.91%)	0.06	-0.00053(-0.83%)	-0.00083(-1.30%)

[Title Page](#)[Abstract](#) [Introduction](#)[Conclusions](#) [References](#)[Tables](#) [Figures](#)[Close](#)[Full Screen / Esc](#)[Printer-friendly Version](#)[Interactive Discussion](#)

Trend analysis of the Aerosol Optical Thickness

J. Yoon et al.

Table 4. Continued.

(i) Mongu			(j) Ouagadougou			
	$\langle \tau \rangle^a$	Unweighted trend/[year]	Weighted trend/[year]	$\langle \tau \rangle$	Unweighted trend/[year]	Weighted trend/[year]
α^b	1.53	+0.01601(+1.05%)	-0.00122(-0.08%)	0.42	+0.01331(+3.14%)	+0.01695(+4.00%)
τ_{440}^c	0.28	+0.01580(+5.70%)	+0.00625(+2.26%)	0.51	+0.01747(+3.42%)	-0.00996(-1.95%)
τ_{675}^c	0.14	+0.00592(+4.30%)	+0.00671(+4.87%)	0.47	-0.00367(-0.78%)	-0.01168(-2.48%)
τ_{870}^c	0.09	+0.00370(+3.99%)	+0.00736(+7.94%)	0.41	+0.01427(+3.48%)	-0.01028(-2.51%)
τ_{1020}^c	0.07	+0.00175(+2.49%)	+0.00582(+8.29%)	0.38	+0.01691(+4.40%)	-0.00720(-1.87%)
(k) SEDE_BOKER			(l) Sevilleta			
α	0.88	+0.00611(+0.69%)	-0.02455(-2.78%)	1.19	+0.00516(+0.43%)	-0.01980(-1.66%)
τ_{440}	0.20	+0.00111(+0.56%)	-0.00427(-2.16%)	0.08	+0.00271(+3.28%)	-0.00313(-3.79%)
τ_{675}	0.14	-0.00007(-0.05%)	-0.00361(-2.60%)	0.05	+0.00096(+1.98%)	-0.00162(-3.35%)
τ_{870}	0.12	+0.00055(+0.45%)	-0.00163(-1.33%)	0.04	+0.00115(+3.01%)	-0.00095(-2.49%)
τ_{1020}	0.11	-0.00032(-0.30%)	-0.00112(-1.05%)	0.03	+0.00124(+3.65%)	+0.00057(+1.68%)

[Title Page](#)[Abstract](#) [Introduction](#)[Conclusions](#) [References](#)[Tables](#) [Figures](#)[Back](#) [Close](#)[Full Screen / Esc](#)[Printer-friendly Version](#)[Interactive Discussion](#)

Trend analysis of the Aerosol Optical Thickness

J. Yoon et al.

Table 4. Continued.

(m) Shirahama			(n) Skukuza		
	< τ > ^a	Unweighted trend/[year]		< τ >	Unweighted trend/[year]
α^b	1.27	+0.01735(+1.37%)	+0.02617(+2.07%)	1.34	+0.00566(+0.42%)
τ_{440}^c	0.31	+0.00082(+0.27%)	+0.00137(+0.44%)	0.23	-0.00113(-0.48%)
τ_{675}^c	0.18	-0.00111(-0.60%)	-0.00012(-0.06%)	0.12	-0.00126(-1.01%)
τ_{870}^c	0.13	-0.00030(-0.22%)	-0.00006(-0.04%)	0.09	-0.00034(-0.39%)
τ_{1020}^c	0.11	-0.00150(-1.35%)	-0.00165(-1.49%)	0.07	-0.00039(-0.54%)
(o) Solar_Village					
α	0.55	-0.02293(-4.16%)	-0.00492(-0.89%)		
τ_{440}	0.31	+0.01881(+6.12%)	+0.01009(+3.29%)		
τ_{675}	0.25	+0.01684(+6.62%)	+0.00541(+2.13%)		
τ_{870}	0.23	+0.01705(+7.35%)	+0.00503(+2.17)		
τ_{1020}	0.23	+0.01373(+6.03%)	+0.00140(+0.62%)		

Title Page

Abstract

Introduction

Conclusions

References

Tables

Figures

◀

▶

Back

Close

Full Screen / Esc

Printer-friendly Version

Interactive Discussion



Trend analysis of the Aerosol Optical Thickness

J. Yoon et al.

Table 5. Climatological averages and statistical parameters for weighted and unweighted trend of Coarse- and Fine-mode dominant AOTs (440, 675, 870, and 1020 nm) at (a) Avignon, (b) Banizoumbou, (c) Beijing, (d) Dakar, (e) GSFC, (f) Ispra, (h) MD_Science_Center, (i) Mongu, (j) Ouagadougou, (k) SEDE_BOKER, (m) Shirahama, (n) Skukuza, and (o) Solar_Village.

Coarse-mode dominant aerosol			Fine-mode dominant aerosol		
	$\langle \tau \rangle$	Unweighted trend/[year]		$\langle \tau \rangle$	Unweighted trend/[year]
(a) Avignon					
τ_{440}	0.15	+0.00364(+2.51%)	+0.00313(+2.16%)	0.18	-0.00026(-0.14%)
τ_{675}	0.09	+0.00207(+2.42%)	+0.00128(+1.50%)	0.09	-0.00058(-0.62%)
τ_{870}	0.07	+0.00122(+1.82%)	+0.00053(+0.79%)	0.06	-0.00095(-1.46%)
τ_{1020}	0.06	+0.00184(+3.14%)	+0.00100(+1.71%)	0.05	-0.00006(-0.11%)
(b) Banizoumbou					
τ_{440}	0.52	-0.00160(-0.31%)	+0.00149(+0.27%)	-	-
τ_{675}	0.47	+0.00040(+0.08%)	+0.00377(+0.80%)	-	-
τ_{870}	0.43	+0.00118(+0.27%)	+0.00462(+1.07%)	-	-
τ_{1020}	0.41	+0.00055(+0.13%)	+0.00374(+0.91%)	-	-
(c) Beijing					
τ_{440}	0.51	-0.00099(-0.19%)	+0.02598(+5.12%)	0.70	+0.02039(+2.90%)
τ_{675}	0.35	+0.00042(+0.12%)	+0.01618(+4.65%)	0.42	+0.01235(+2.97%)
τ_{870}	0.28	+0.00137(+0.49%)	+0.01189(+4.25%)	0.29	+0.00921(+3.15%)
τ_{1020}	0.25	+0.00157(+0.64%)	+0.00979(+3.97%)	0.23	+0.00769(+3.27%)

- [Title Page](#)
- [Abstract](#) | [Introduction](#)
- [Conclusions](#) | [References](#)
- [Tables](#) | [Figures](#)
- [◀](#) | [▶](#)
- [◀](#) | [▶](#)
- [Back](#) | [Close](#)
- [Full Screen / Esc](#)
- [Printer-friendly Version](#)
- [Interactive Discussion](#)



Trend analysis of the Aerosol Optical Thickness

J. Yoon et al.

Table 5. Continued.

Coarse-mode dominant aerosol			Fine-mode dominant aerosol		
	$\langle \tau \rangle$	Unweighted trend/[year]		$\langle \tau \rangle$	Unweighted trend/[year]
(d) Dakar					
τ_{440}	0.46	-0.01223(-2.69 %)	-0.00669(-1.47 %)	-	-
τ_{675}	0.41	-0.00990(-2.44 %)	-0.00225(-0.56 %)	-	-
τ_{870}	0.38	-0.00754(-2.01 %)	+0.00121(+0.32 %)	-	-
τ_{1020}	0.36	-0.00708(-1.99 %)	+0.00231(+0.65 %)	-	-
(e) GSFC					
τ_{440}	0.14	-0.00340(-2.51 %)	-0.00027(-0.20 %)	0.22	-0.00025(-0.11 %)
τ_{675}	0.07	-0.00293(-3.94 %)	-0.00014(-0.18 %)	0.11	-0.00040(-0.37 %)
τ_{870}	0.06	-0.00260(-4.47 %)	+0.00011(+0.19 %)	0.07	-0.00024(-0.35 %)
τ_{1020}	0.05	-0.00231(-4.59 %)	+0.00029(+0.57 %)	0.05	-0.00007(-0.14 %)
(f) Ispra					
τ_{440}	0.16	+0.00389(+2.36 %)	-0.00174(-1.05 %)	0.29	-0.00324(-1.12 %)
τ_{675}	0.10	+0.00166(+1.67 %)	-0.00257(-2.58 %)	0.15	-0.00183(-1.20 %)
τ_{870}	0.08	+0.00149(+1.90 %)	-0.00151(-1.92 %)	0.10	-0.00077(-0.76 %)
τ_{1020}	0.07	+0.00113(+1.65 %)	-0.00151(-2.20 %)	0.08	-0.00069(-0.87 %)



Trend analysis of the Aerosol Optical Thickness

J. Yoon et al.

Table 5. Continued.

Coarse-mode dominant aerosol			Fine-mode dominant aerosol		
	$\langle \tau \rangle$	Unweighted trend/[year]	$\langle \tau \rangle$	Unweighted trend/[year]	Weighted trend/[year]
(h) MD_Science.Center					
τ_{440}	0.14	+0.00073(+0.52 %)	+0.00202(+1.45 %)	0.24	-0.00135(-0.56 %)
τ_{675}	0.07	+0.00031(+0.42 %)	+0.00076(+1.01 %)	0.12	-0.00058(-0.49 %)
τ_{870}	0.06	+0.00057(+1.02 %)	+0.00106(+1.90 %)	0.08	+0.00006(+0.08 %)
τ_{1020}	0.05	+0.00001(+0.03 %)	+0.00017(+0.33 %)	0.06	-0.00029(-0.49 %)
(i) Mongu					
τ_{440}	0.20	-0.00608(-3.01 %)	-0.00037(-0.18 %)	0.27	+0.01648(+6.13 %)
τ_{675}	0.12	-0.00475(-4.07 %)	+0.00042(+0.36 %)	0.13	+0.00641(+4.94 %)
τ_{870}	0.09	-0.00338(-3.69 %)	+0.00144(+1.57 %)	0.08	+0.00415(+4.91 %)
τ_{1020}	0.08	-0.00378(-4.93 %)	+0.00109(+1.43 %)	0.06	+0.00223(+3.59 %)
(j) Ouagadougou					
τ_{440}	0.51	+0.01764(+3.44 %)	-0.00953(-1.86 %)	-	-
τ_{675}	0.47	-0.00333(-0.71 %)	-0.01259(-2.67 %)	-	-
τ_{870}	0.41	+0.01469(+3.57 %)	-0.01133(-2.76 %)	-	-
τ_{1020}	0.39	+0.01734(+4.50 %)	-0.00830(-2.15 %)	-	-

Table 5. Continued.

Coarse-mode dominant aerosol			Fine-mode dominant aerosol		
	< τ >	Unweighted trend/[year]	< τ >	Unweighted trend/[year]	Weighted trend/[year]
(k) SEDE_BOKER					
τ_{440}	0.19	+0.00162(+0.83 %)	-0.00445(-2.30 %)	0.13	-0.00014(-0.11 %)
τ_{675}	0.14	+0.00021(+0.15 %)	-0.00452(-3.26 %)	0.08	-0.00016(-0.21 %)
τ_{870}	0.12	+0.00075(+0.61 %)	-0.00305(-2.46 %)	0.07	+0.00083(+1.27 %)
τ_{1020}	0.11	-0.00030(-0.27 %)	-0.00342(-3.15 %)	0.05	+0.00025(+0.49 %)
(m) Shirahama					
τ_{440}	0.23	+0.00604(+2.62 %)	+0.00423(+1.83 %)	0.31	+0.00137(+0.44 %)
τ_{675}	0.15	+0.00190(+1.29 %)	+0.00210(+1.43 %)	0.17	-0.00100(-0.57 %)
τ_{870}	0.12	+0.00165(+1.40 %)	+0.00205(+1.74 %)	0.12	-0.00035(-0.29 %)
τ_{1020}	0.10	-0.00006(-0.06 %)	+0.00047(+0.47 %)	0.10	-0.00156(-1.64 %)
(n) Skukuza					
τ_{440}	0.14	+0.00119(+0.83 %)	+0.00044(+0.31 %)	0.23	-0.00113(-0.49 %)
τ_{675}	0.09	-0.00070(-0.80 %)	-0.00095(-1.08 %)	0.12	-0.00124(-1.03 %)
τ_{870}	0.07	-0.00035(-0.51 %)	-0.00005(-0.08 %)	0.08	-0.00030(-0.36 %)
τ_{1020}	0.06	-0.00067(-1.11 %)	-0.00039(-0.64 %)	0.07	-0.00033(-0.50 %)
(o) Solar_Village					
τ_{440}	0.31	+0.01888(+6.15 %)	+0.01042(+3.39 %)	—	—
τ_{675}	0.25	+0.01682(+6.60 %)	+0.00573(+2.25 %)	—	—
τ_{870}	0.23	+0.01697(+7.31 %)	+0.00530(+2.28 %)	—	—
τ_{1020}	0.23	+0.01367(+6.00 %)	+0.00173(+0.76 %)	—	—

Trend analysis of the Aerosol Optical Thickness

J. Yoon et al.

[Title Page](#)[Abstract](#)[Introduction](#)[Conclusions](#)[References](#)[Tables](#)[Figures](#)[|◀](#)[▶|](#)[◀](#)[▶](#)[Back](#)[Close](#)[Full Screen / Esc](#)[Printer-friendly Version](#)[Interactive Discussion](#)

Trend analysis of the Aerosol Optical Thickness

J. Yoon et al.

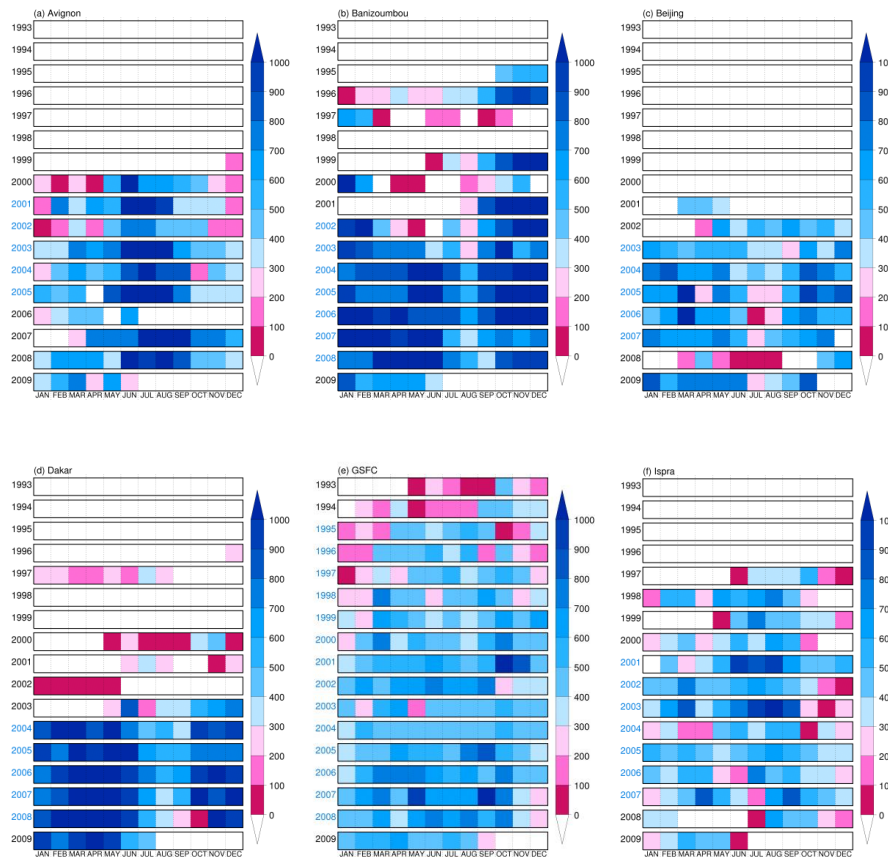


Fig. 1. The monthly observation numbers at the AEROET stations: **(a)** Avignon, **(b)** Banizoumbou, **(c)** Beijing, **(d)** Dakar, **(e)** GSFC, **(f)** Ispra, **(g)** Mauna.Loa, **(h)** MD_Science_Center, **(i)** Mongu, **(j)** Ouagadougou, **(k)** SEDE_BOKER, **(l)** Sevilleta, **(m)** Shirahama, **(n)** Skukuza, and **(o)** Solar_Village since 1993. The research period for each station is shown by the blue years at vertical axis.

[Title Page](#)

[Abstract](#)

[Introduction](#)

[Conclusions](#)

[References](#)

[Tables](#)

[Figures](#)

◀

▶

◀

▶

[Back](#)

[Close](#)

[Full Screen / Esc](#)

[Printer-friendly Version](#)

[Interactive Discussion](#)

Trend analysis of the Aerosol Optical Thickness

J. Yoon et al.

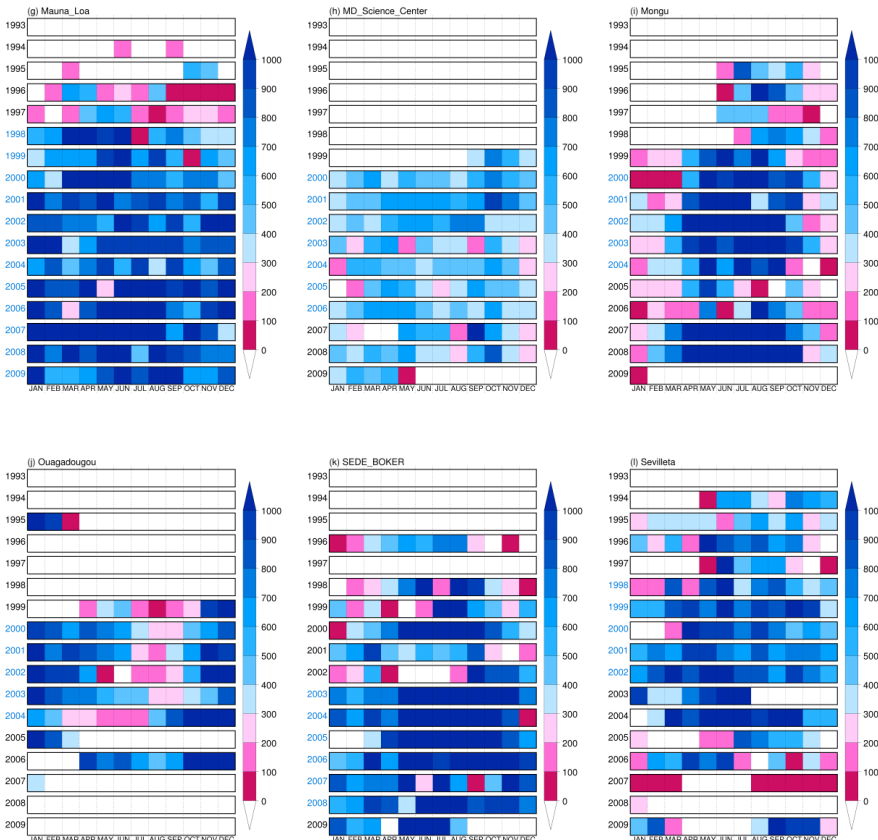


Fig. 1. Continued.

Title Page

Abstract

Introduction

Conclusions

References

Tables

Figures



Full Screen / Esc

Printer-friendly Version

Interactive Discussion

Trend analysis of the Aerosol Optical Thickness

J. Yoon et al.

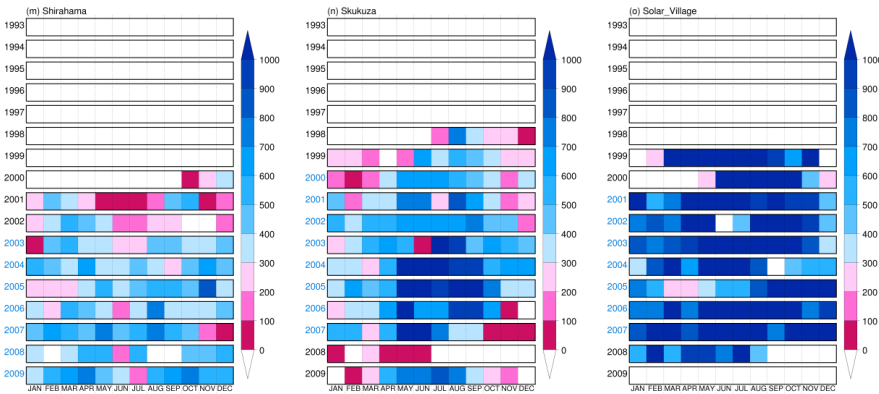


Fig. 1. Continued.

5369

Trend analysis of the Aerosol Optical Thickness

J. Yoon et al.

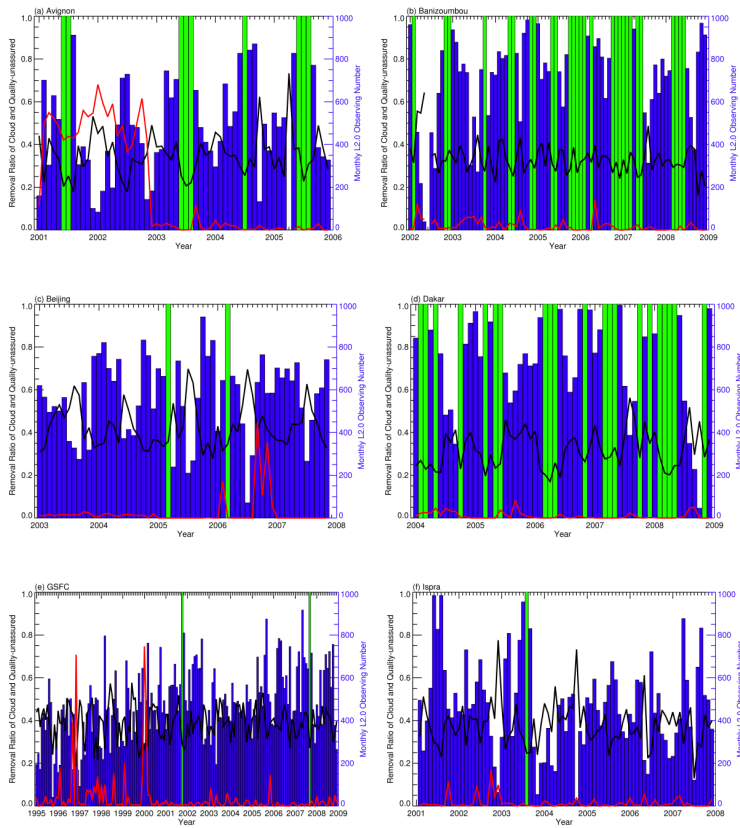


Fig. 2. The removal ratio of cloud (black line) and quality-unassured (red line) cases to Level 2.0 data (blue bar) within each of research period at the AERONET stations: **(a)** Avignon, **(b)** Banizoumbou, **(c)** Beijing, **(d)** Dakar, **(e)** GSFC, **(f)** Ispra, **(g)** Mauna_Loa, **(h)** MD_Science_Center, **(i)** Mongu, **(j)** Ouagadougou, **(k)** SEDE_BOKER, **(l)** Sevilleta, **(m)** Shirahama, **(n)** Skukuza, and **(o)** Solar_Village. Green bars mean that the monthly observation numbers are over 1000 times.

Trend analysis of the Aerosol Optical Thickness

J. Yoon et al.

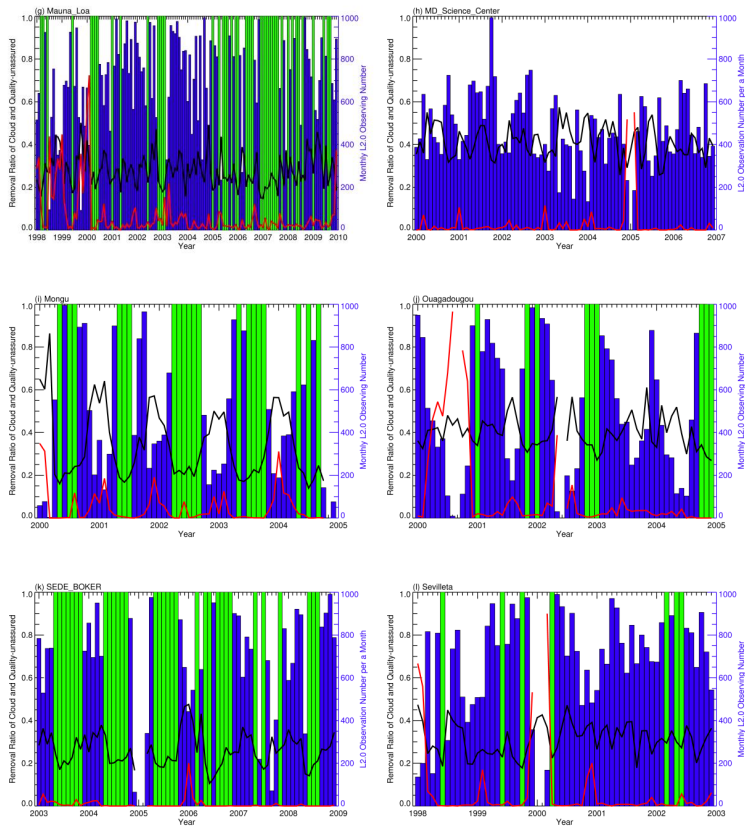


Fig. 2. Continued.

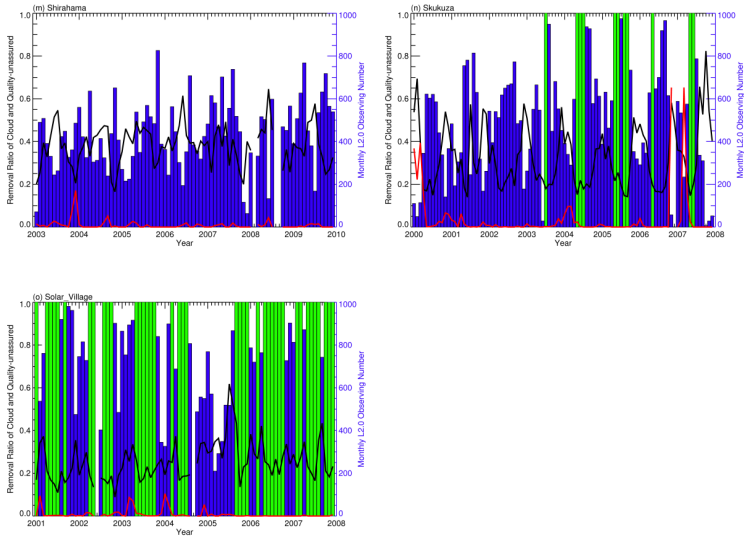


Fig. 2. Continued.

Trend analysis of the Aerosol Optical Thickness

J. Yoon et al.

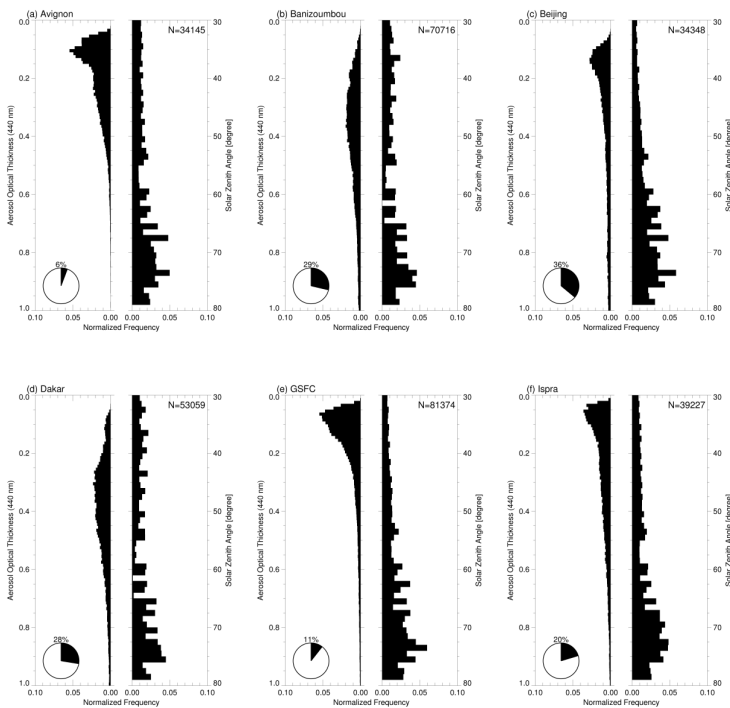


Fig. 3. Normalized frequency of Aerosol Optical Thickness at 440 nm (τ_{440}) and solar zenith angle (θ) to total observation number (N) at the AERONET stations: **(a)** Avignon, **(b)** Bani-zoumbou, **(c)** Beijing, **(d)** Dakar, **(e)** GSFC, **(f)** Ispra, **(g)** Mauna_Loa, **(h)** MD_Science_Center, **(i)** Mongu, **(j)** Ouagadougou, **(k)** SEDE_BOKER, **(l)** Sevilleta, **(m)** Shirahama, **(n)** Skukuza, and **(o)** Solar_Village. The bin sizes for τ_{440} and θ are 0.01 and 1.0°, respectively. The circle diagram on the lower-left hand means the percentage of AERONET level 2.0 inversion data (e.g. volume size distribution and Single Scattering Albedo (SSA)) to total observations. The AERONET inversion data are provided under the criteria; $\tau_{440} > 0.4$ and $\theta > 50^\circ$.

Trend analysis of the Aerosol Optical Thickness

J. Yoon et al.

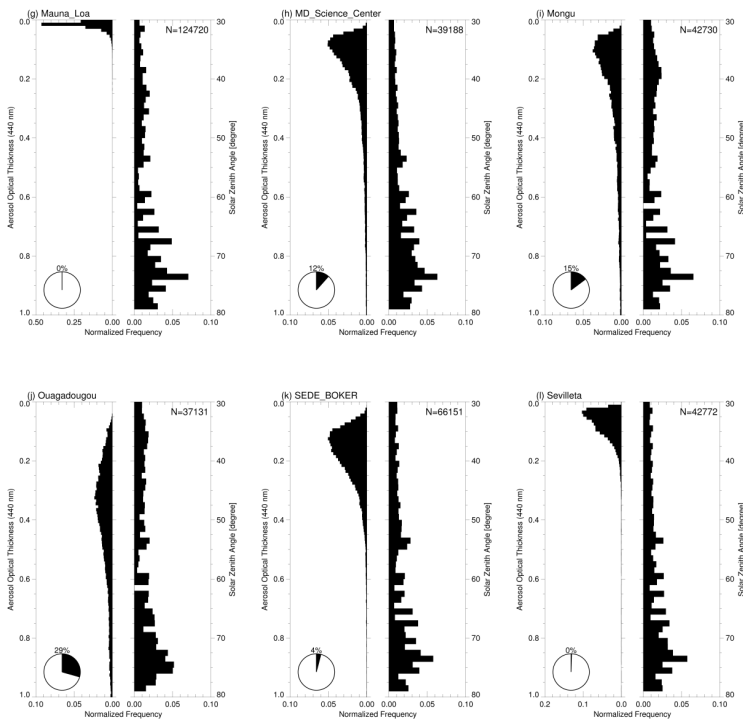


Fig. 3. Continued.

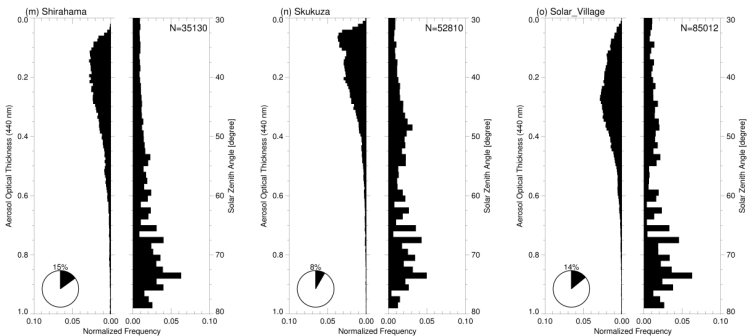


Fig. 3. Continued.

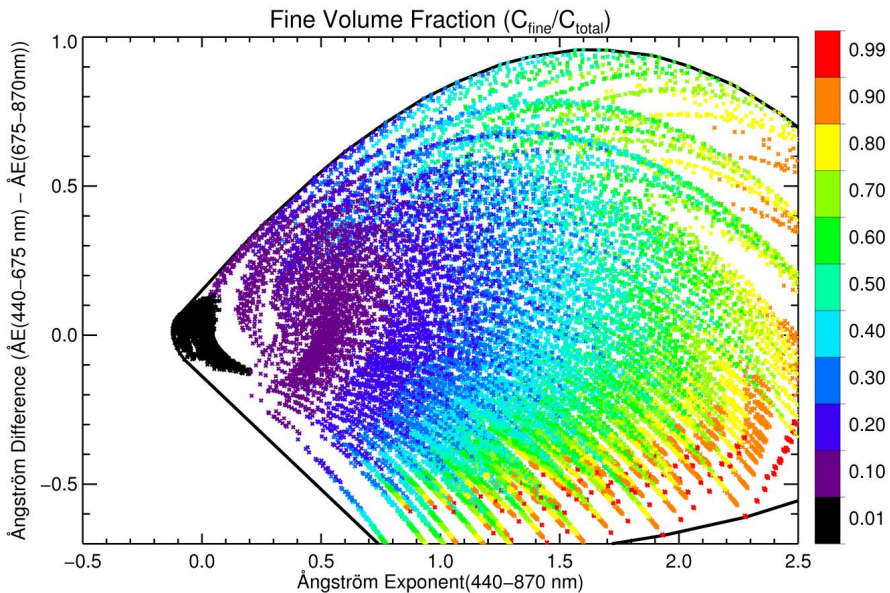


Fig. 4. Simulations of the fine volume fraction as a function of Ångström Exponent (440–870 nm) and Ångström Exponent Difference ($\Delta E(440\text{--}675\text{ nm}) - \Delta E(675\text{--}870\text{ nm})$) using Mie theory with all combinations of volume median radius, standard deviation, refractive indices, and fine volume fractions shown Table 2.

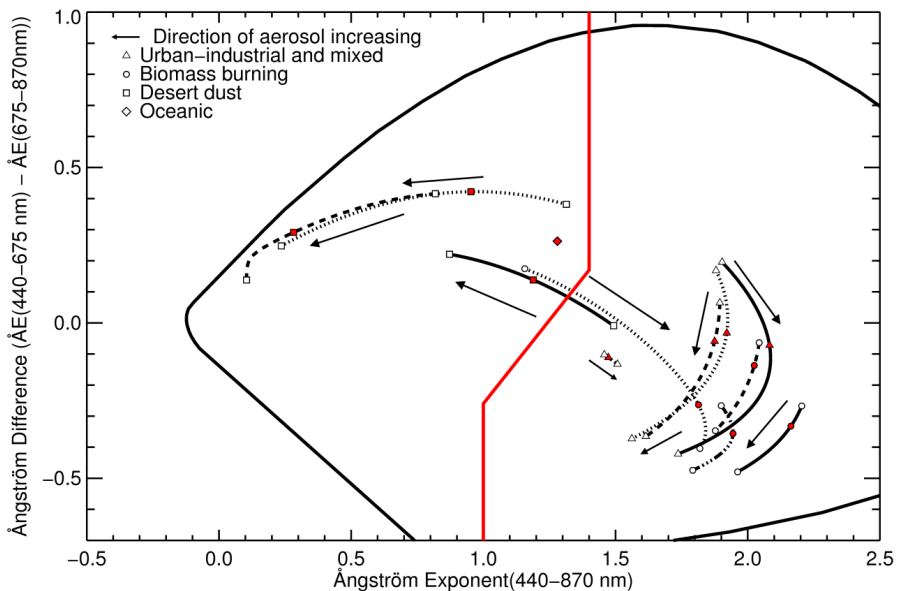


Fig. 5. Mie simulations (solid, dotted, dashed, dash-dot-dot lines) for the typical aerosols (urban-industrial and mixed, biomass burning, desert dust, oceanic) depending on an increase of aerosol loading in Dubovik et al. (2001) shown Table 3. The red spot and red line represent the simulations for AOT average of the typical aerosols and the classification line for two aerosol types (fine- and coarse-mode dominant aerosols), respectively.

Trend analysis of the Aerosol Optical Thickness

J. Yoon et al.

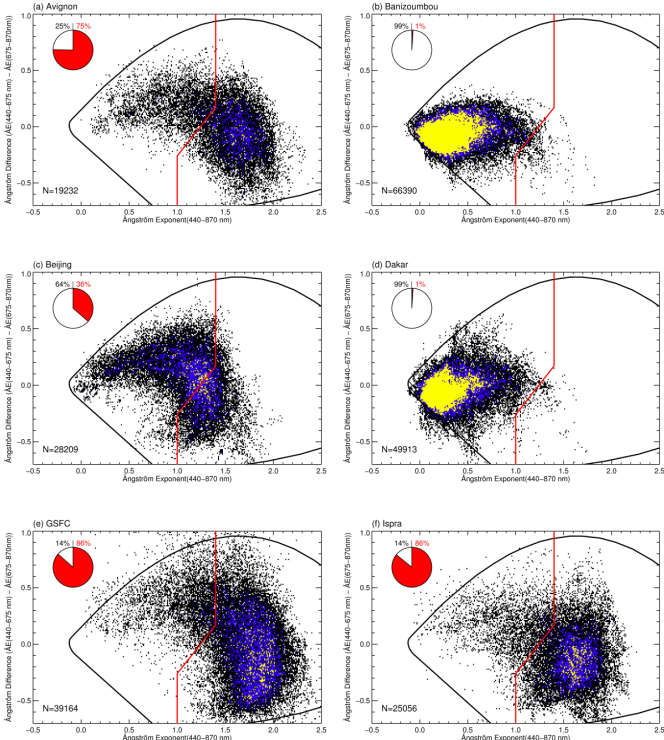


Fig. 6. Applications of the classification method to the AERONET datasets at (a) Avignon, (b) Banizoumbou, (c) Beijing, (d) Dakar, (e) GSFC, (f) Ispra, (g) Mauna_Loa, (h) MD_Science_Center, (i) Mongu, (j) Ouagadougou, (k) SEDE_BOKER, (l) Sevilleta, (m) Shirahama, (n) Skukuza, and (o) Solar_Village, which are characterized by two aerosol types as fine- and coarse-mode dominant aerosols. The circle diagram on the upper-left hand means the percentage of fine-(red) and coarse-mode (black) dominant aerosols to total observations (N). To avoid large errors in Ångström Exponent and Ångström Exponent Difference from low AOTs, only AERONET level 2.0 data with AOT (440 nm) > 0.15 were used.

Title Page

Abstract

Introduction

Conclusions

References

Tables

Figures

◀

▶

◀

▶

Back

Close

Full Screen / Esc

Printer-friendly Version

Interactive Discussion



Trend analysis of the Aerosol Optical Thickness

J. Yoon et al.

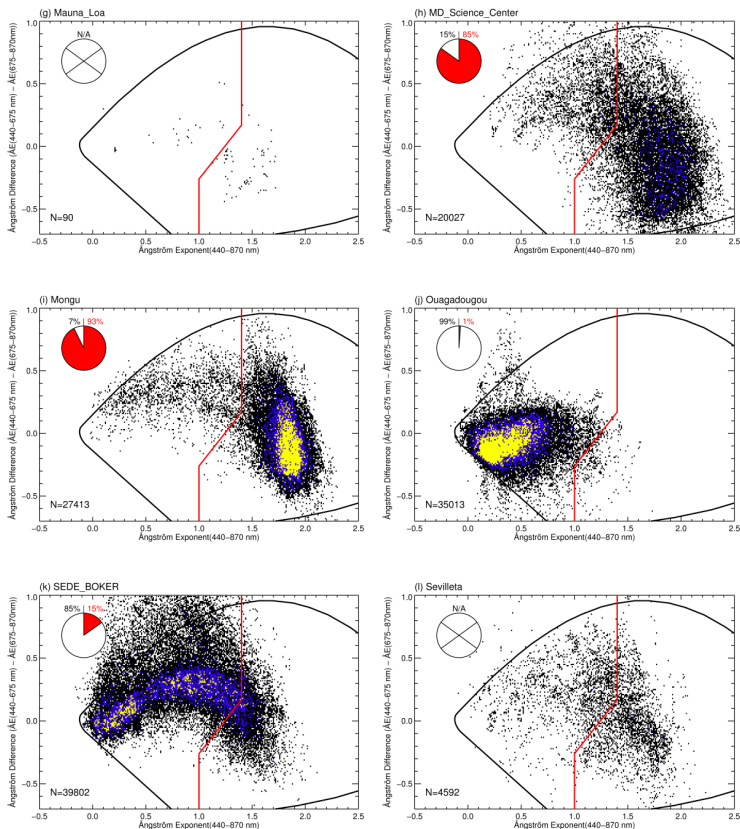


Fig. 6. Continued.

Fig. 6. Continued.

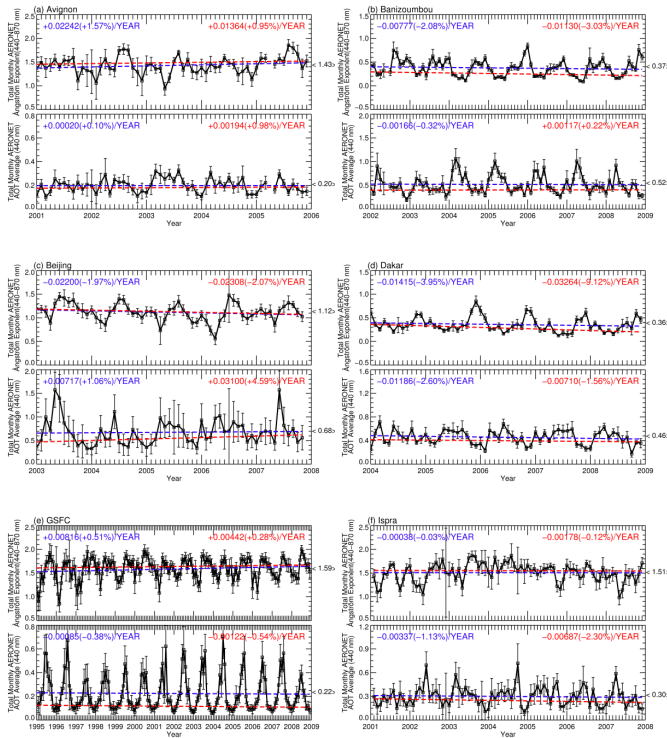


Fig. 7. Total averages (black one enclosed with parentheses at right vertical axis), temporal unweighted (blue one on the left upper part), and weighted (red one on the right upper part) trends of Ångström Exponent (440–870 nm) and AOT (440 nm) at the AERONET stations: **(a)** Avignon, **(b)** Banizoumbou, **(c)** Beijing, **(d)** Dakar, **(e)** GSFC, **(f)** Ispra, **(g)** Mauna_Loa, **(h)** MD_Science_Center, **(i)** Mongu, **(j)** Ouagadougou, **(k)** SEDE_BOKER, **(l)** Sevilleta, **(m)** Shirahama, **(n)** Skukuza, and **(o)** Solar_Village. The error bar means the 10 times of the standard error, which are used for the weighted trend analysis.

Trend analysis of the Aerosol Optical Thickness

J. Yoon et al.

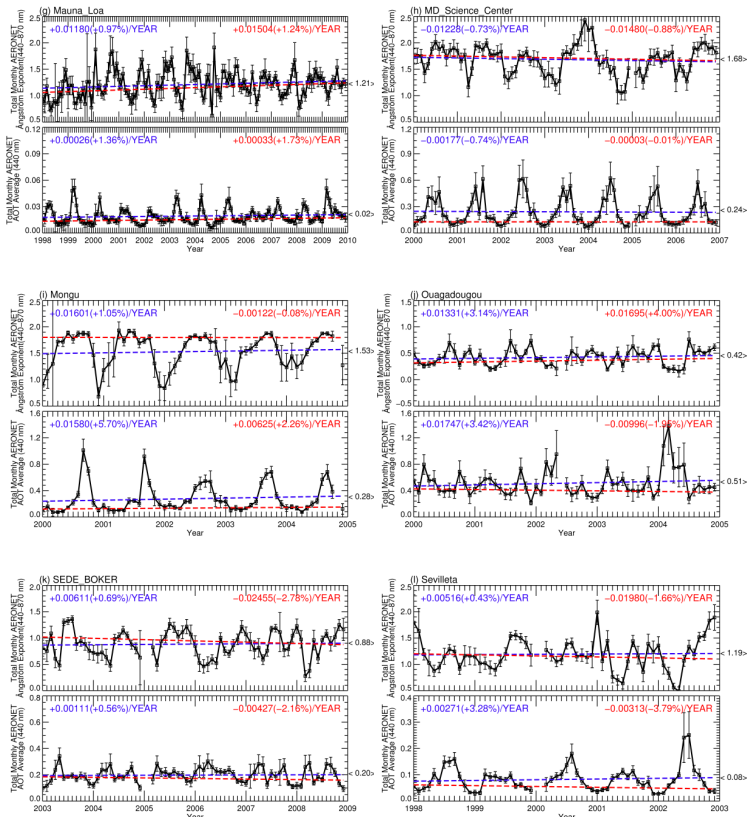


Fig. 7. Continued.

Trend analysis of the Aerosol Optical Thickness

J. Yoon et al.

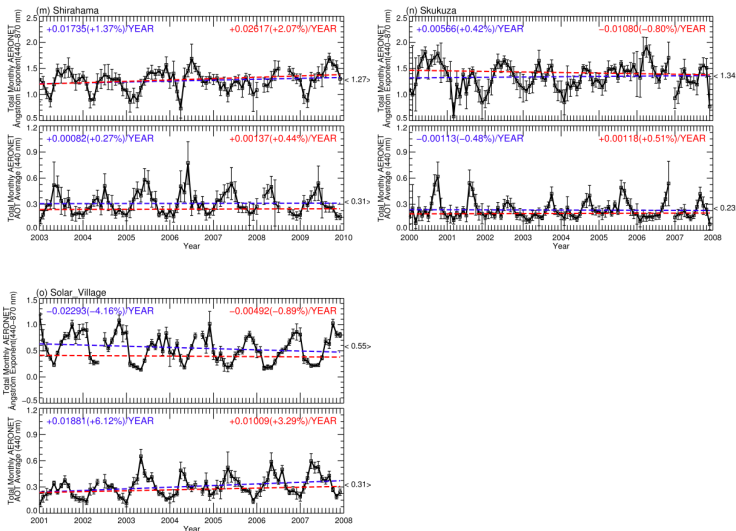


Fig. 7. Continued.

[Title Page](#)

[Abstract](#)

[Introduction](#)

[Conclusions](#)

[References](#)

[Tables](#)

[Figures](#)

◀

▶

◀

▶

[Back](#) [Close](#)

[Full Screen / Esc](#)

[Printer-friendly Version](#)

[Interactive Discussion](#)



Trend analysis of the Aerosol Optical Thickness

J. Yoon et al.



Fig. 8. The weighted trends of Ångström Exponent (440–870 nm) (left square) and AOT at 440 nm (right diamond) in percent at the major stations were indicated except (**a**) Avignon (+0.95%/year and +0.98%/year) over Western Europe, (**h**) MD_Science_Center (−0.88%/year and −0.01%/year) over North America, and (**j**) Ouagadougou (+4.00%/year and −1.95%/year, respectively) over West Africa.

[Title Page](#)

[Abstract](#)

[Introduction](#)

[Conclusions](#)

[References](#)

[Tables](#)

[Figures](#)

[|◀](#)

[▶|](#)

[◀](#)

[▶](#)

[Back](#)

[Close](#)

[Full Screen / Esc](#)

[Printer-friendly Version](#)

[Interactive Discussion](#)

Trend analysis of the Aerosol Optical Thickness

J. Yoon et al.

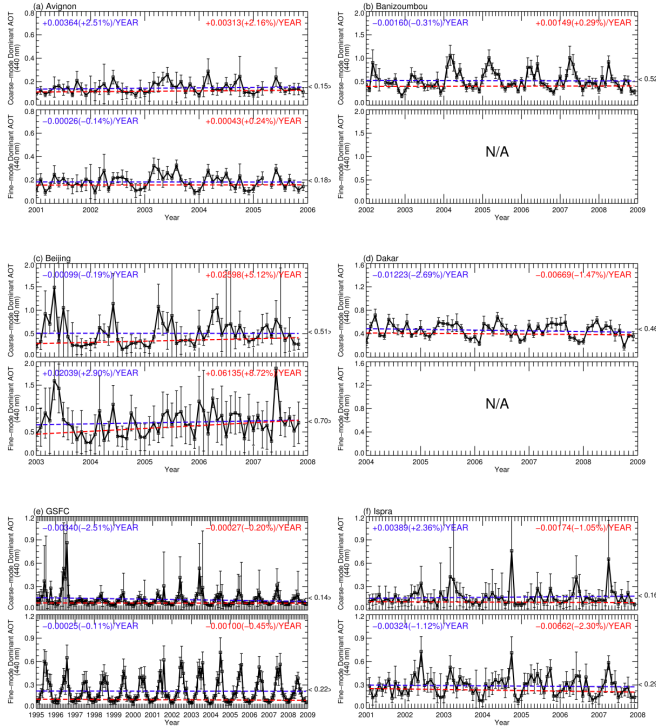


Fig. 9. Total averages (black one enclosed with parentheses at right vertical axis), temporal unweighted (blue one on the left upper part), and weighted (red one on the right upper part) trends of coarse- and fine-mode dominant AOT (440 nm) at the AERONET stations: **(a)** Avignon, **(b)** Banizoumbou, **(c)** Beijing, **(d)** Dakar, **(e)** GSFC, **(f)** Ispra, **(h)** MD_Science_Center, **(i)** Mongu, **(j)** Ouagadougou, **(k)** SEDE_BOKER, **(m)** Shirahama, **(n)** Skukuza, and **(o)** Solar_Village. The error bar means the 10 times of the standard error, which are used for the weighted trend analysis. Trend analysis of fine-mode dominant AOT is non-applicable (N/A) at **(b)** Banizoumbou, **(d)** Dakar, **(j)** Ouagadougou, and **(o)** Solar_Village.

Trend analysis of the Aerosol Optical Thickness

J. Yoon et al.

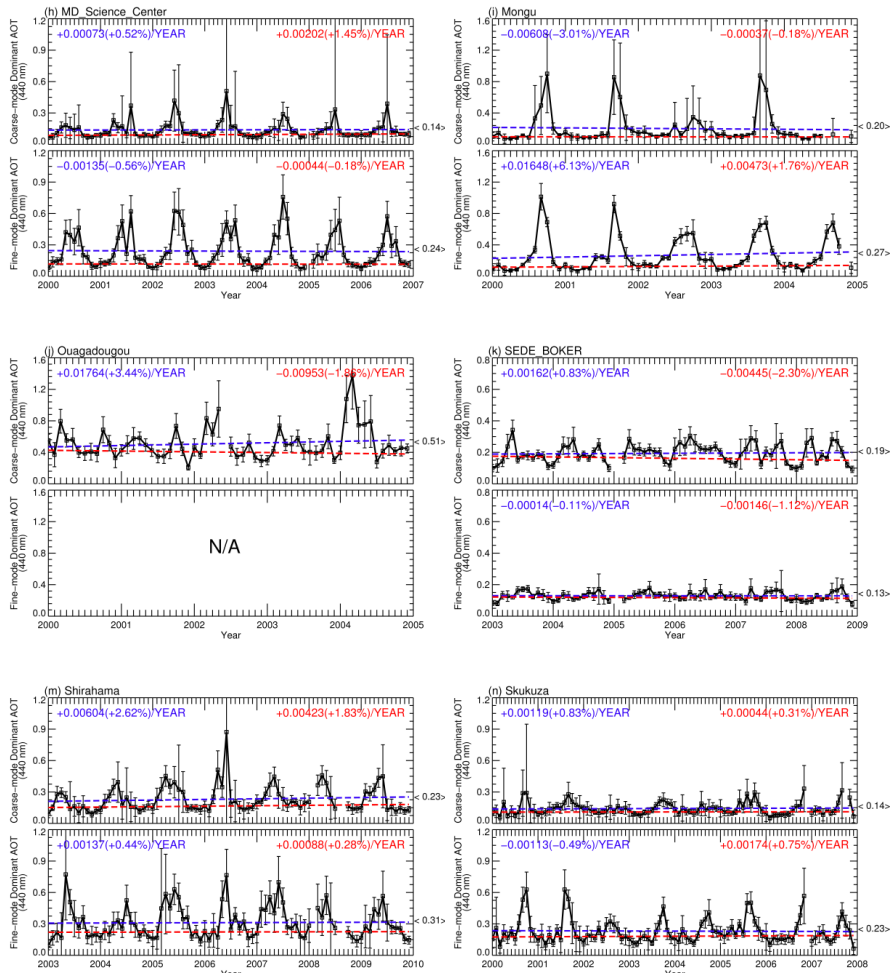


Fig. 9. Continued.

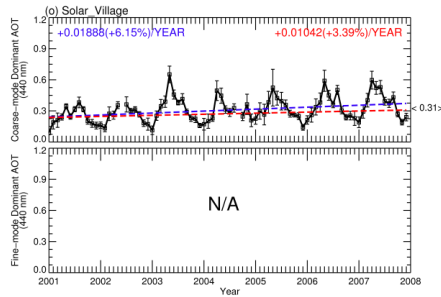


Fig. 9. Continued.

Discussion Paper | Discussion Paper | Discussion Paper | Discussion Paper

Discussion Paper

Discussion Paper

Discussion Paper

Title Page	
Abstract	Introduction
Conclusions	References
Tables	Figures
◀	▶
◀	▶
Back	Close
Full Screen / Esc	
Printer-friendly Version	
Interactive Discussion	



Trend analysis of the Aerosol Optical Thickness

J. Yoon et al.

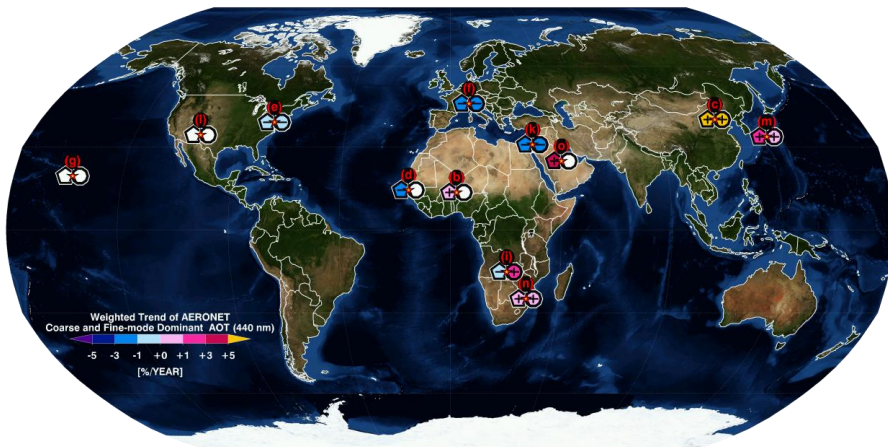


Fig. 10. The weighted trends of coarse- (left pentagon) and fine-mode (right circle) dominant AOT (440 nm) in percent at the major stations were indicated except (a) Avignon (+2.16%/year and +0.24%/year) over Western Europe, (h) MD_Science_Center (+1.45%/year and -0.18%/year) over North America, and (i) Ouagadougou (-1.86%/year and non-applicable, respectively) over West Africa. Non-applicable cases are shown as a white blank.

[Title Page](#)

[Abstract](#)

[Introduction](#)

[Conclusions](#)

[References](#)

[Tables](#)

[Figures](#)

◀

▶

[Back](#)

[Close](#)

[Full Screen / Esc](#)

[Printer-friendly Version](#)

[Interactive Discussion](#)